NASA Technical Memorandum 106992

CVD Silicon Carbide Monofilament Reinforced $SrO\text{-}Al_2O_3\text{-}2SiO_2$ (SAS) Glass-Ceramic Composites

Narottam P. Bansal
Lewis Research Center
Cleveland, Ohio

August 1995

National Aeronautics and
Space Administration

CVD Silicon Carbide Monofilament Reinforced $SrO\text{-}Al_2O_3\text{-}2SiO_2$ (SAS) Glass-Ceramic Composites

Narottam P. Bansal
National Aeronautics and Space Administration
Lewis Research Center
Cleveland, Ohio 44135

ABSTRACT

Unidirectional CVD SiC fiber-reinforced $SrO.Al_2O_3.2SiO_2$ (SAS) glass-ceramic matrix composites have been fabricated by hot pressing at various combinations of temperature, pressure and time. Both carbon-rich surface coated SCS-6 and uncoated SCS-0 fibers were used as reinforcements. Almost fully dense composites have been obtained. Monoclinic celsian, $SrAl_2Si_2O_8$, was the only crystalline phase observed in the matrix from x-ray diffraction. During three point flexure testing of composites, a test span to thickness ratio of $\sim$25 or greater was necessary to avoid sample delamination. Strong and tough SCS-6/SAS composites having a first matrix crack stress of $\sim$ 300 MPa and an ultimate bend strength of $\sim$ 825 MPa were fabricated. No chemical reaction between the SCS-6 fibers and the SAS matrix was observed after high temperature processing. The uncoated SCS-0 fiber-reinforced SAS composites showed only limited improvement in strength over SAS monolithic. The SCS-0/SAS composite having a fiber volume fraction of 0.24 and hot pressed at 1400°C exhibited a first matrix cracking stress of $\sim 231 \pm 20$ MPa and ultimate strength of 265 ± 17 MPa. From fiber push-out tests, the fiber/matrix interfacial debonding strength (τ_{debond}) and frictional sliding stress ($\tau_{friction}$) in the SCS-6/SAS system were evaluated to be $\sim 6.7 \pm 2.3$ MPa and 4.3 ± 0.6 MPa, respectively, indicating a weak interface. However, for the SCS-0/SAS composite, much higher values of $\sim 17.5 \pm 2.7$ MPa for τ_{debond} and 11.3 ± 1.6 MPa for $\tau_{friction}$ respectively, were observed; some of the fibers were so strongly bonded to the matrix that they could not be pushed out. Examination of fracture surfaces revealed limited short pull-out length of SCS-0 fibers. The applicability of various micromechanical models for predicting the values of first matrix cracking stress and ultimate strength of these composites were examined.

1. INTRODUCTION

Strong, tough, and environmentally stable fiber-reinforced composites (FRC) are needed for various high temperature structural applications in the aerospace and other industries. Various glass and glass-ceramics are being used as matrices for fiber-reinforced composites. However, $BaO.Al_2O_3.2SiO_2$ (BAS) and $SrO.Al_2O_3.2SiO_2$ (SAS) glass ceramics having monoclinic celsian as the crystalline phase are the most refractory having melting points of > 1700°C. They also have a low thermal expansion coefficient of ~2.5 x 10^{-6}/°C resulting in potential for good thermal shock resistance. Celsian is also oxidation resistant, phase stable up to ~1600°C for BAS and up to the melting point for SAS. BAS and SAS glass-ceramics, therefore, are being studied as matrix materials for fabrication of fiber-reinforced composites at NASA Lewis Research Center. Processing and properties of CVD SiC fiber-reinforced BAS glass-ceramic matrix composites have been described earlier[1-3]. Results of a study on CVD SiC monofilament reinforced SAS glass-ceramic matrix composites are being presented here.

The long term objective of this research project is the development of strong, tough, and environmentally stable fiber-reinforced glass-ceramic matrix composites for high temperature structural applications in the aerospace industry. The primary objective of the present study was to establish the temperature, pressure, and time of hot pressing which would yield a strong, tough, and almost fully dense composites without degradation of the constituent fibers and the matrix properties. Other objectives were to study the effects of fiber surface coating on the fiber/matrix interface and the composite properties, and also to examine the applicability of various theoretical models in predicting the matrix microcracking stress and ultimate strength of the composites. Unidirectional fiber-reinforced composites were fabricated by hot pressing in vacuum using a glass-ceramic approach to take advantage of the viscous flow of glass resulting in almost fully dense composites. Flexural strengths of the resulting composites were measured in 3-point bending mode and the fiber/matrix interfacial shear strengths were evaluated by a fiber push-out method.

2. MATERIALS AND EXPERIMENTAL METHODS

2.1. Materials

Strontium aluminosilicate glass of stoichiometric celsian composition, $SrO.Al_2O_3.2SiO_2$ (SAS), was used as precursor to the matrix. The glass was melted at ~2000°C in a continuous

electric melter with Mo electrodes using laboratory grade $SrCO_3$, Al_2O_3, and SiO_2. Homogeneous and clear glass flakes were produced by quenching the melt between water-cooled metallic rollers. Attrition milling of the glass frit using alumina or zirconia media in the presence of Darvan as a surfactant resulted in glass powder having an average particle size of $\sim 2.5\ \mu m$. From wet chemical analysis, the composition of the glass powder was determined in weight percent to be 33.7 SrO, 31.5 Al_2O_3, 33.8 SiO_2, 0.12 Na_2O, and 0.86 BaO. The Mo was estimated at 0.01 wt % MoO_3 by a spectrographic technique. The batch composition in weight percent was 31.8 SrO, 31.3 Al_2O_3, and 36.9 SiO_2, which corresponds to stoichiometric celsian.

Continuous CVD SiC monofilaments SCS-0 and SCS-6 from Textron Specialty Materials, having a nominal diameter of $\sim 140\ \mu m$, were used as the reinforcements. The schematics of the cross-sections and the surface regions of the fibers are shown in Fig. 1. These fibers are produced by chemical vapor deposition of SiC onto a pyrolytic graphite-coated carbon core having diameter of 37 μm. The fiber is made up of two distinct zones. The inner zone consists[4] of carbon-rich β-SiC columnar grains extending in the radial direction with $< 111 >$ preferred orientation and lengths of a few micrometers. The outer zone consists of nearly stoichiometric β-SiC grains. The average grain diameter changes from ~ 50 nm in the inner zone to ~ 100 nm in the outer zone[4]. The SCS-0 fiber has no surface coating whereas the surface of the SCS-6 fiber is coated with dual carbon-rich SiC layers (Fig. 1). At room temperature these fibers typically have an elastic modulus of ~ 390-400 GPa and tensile strengths of ~ 1.8 and 3.9 GPa for the SCS-0 and SCS-6 fibers, respectively. The average axial thermal expansion coefficient of these fibers, from room temperature to 1000°C, is $\sim 4.4 \times 10^{-6}$/°C.

2.2. Composite Fabrication

Unidirectional SCS-0/SAS and SCS-6/SAS panels $\sim 112.5 \times 50 \times 1.25$ mm (4½" x 2" x 0.05") were fabricated using a glass-ceramic approach to take advantage of viscous flow of the glass during hot pressing. Details of this method are described elsewhere[1-3]. An aqueous slurry of SAS glass powder along with organic additives was cast into tapes using a Doctor blade and allowed to dry in ambient atmosphere. The dry tape, ~ 0.15 mm thick, was cut to size. The fiber mats were prepared by winding continuous SiC fibers on a drum with a spacing of 41 fibers per cm and cut to size. Adhesive tape was used to hold the fibers in place. Matrix tapes

and fiber mats were alternately stacked up in the desired orientation and warm pressed. The resulting "green" composite was wrapped in Mo foil and then in grafoil, and hot pressed under vacuum in a graphite die. Pressing variables were temperature, pressure and time. The fugitive binder was burned out in situ in the hot press by holding at ~400°C. During hot pressing pressure was first applied at 900°C. The resulting FRC panels were surface polished and sliced into flexure test bars using a high speed diamond cutting wheel.

2.3. Characterization

Microstructures of the polished cross-sections as well as fracture surfaces were observed in an optical microscope as well as in a JEOL JSM-840A scanning electron microscope (SEM). X-ray dot mapping of various elements in the fiber/matrix interface region was carried out using a Kevex Delta class analyzer. Densities were measured by the Archimedes method as well as from specimen dimensions and weight. The fiber volume fraction, V_f, in the composite was determined from

$$V_f = N_f \pi D_f^2 / 4Wd \quad (1)$$

where N_f is the number of fibers, D_f is the fiber diameter assumed to be 142 μm, and W and d are the width and thickness of the specimen, respectively. The crystalline phases formed in the glass-ceramic matrix were identified from powder x-ray diffraction (XRD) patterns recorded at room temperature using a step scan procedure (0.03°/2θ step, count time 0.5 s) on a Philips ADP-3600 automated powder diffractometer equipped with a crystal monochromator and employing copper K_α radiation. Thermogravimetric analysis (TGA) was carried out at a heating rate of 5°C/min under flowing air from room temperature to 1500°C using a Perkin-Elmer TGA-7 system which was interfaced with a computerized data acquisition and analysis system. Mechanical properties of the composites were determined from stress-strain curves recorded in three-point flexure rather than four-point bending because tensile fracture rather than interlaminar shear failure is the more likely failure mode in three-point bend tests. An Instron machine at a crosshead speed of 0.127 cm/min (0.05 in./min) was used. In one case, the effect of test span length (L) to sample thickness (d) ratio on first matrix cracking stress and ultimate strength of the composite was also investigated. A value of L/d >25 was used in subsequent

strength measurements with span length of the lower rollers of 3.75 cm (1.5 in.). The first matrix cracking stress and the elastic modulus of the composites were determined from strain gauges glued to the tensile surface of the test bars. A discontinuous jump in strain in the load vs. strain plot indicated matrix cracking. Matrix cracking was also indicated by discontunity in the load vs. time output of a chart recorder. Values of first matrix cracking stress obtained from the two techniques were in good agreement. Elastic modulus was determined from the linear portion of the load vs. strain curve up to the first matrix cracking load. The SAS monolithic samples were tested in four-point flexure.

Fiber/matrix interfacial shear strength (ISS) was determined from a fiber push-out test using thin polished sections of the composites cut normal to the fiber axis. The indenter, a 100 μm diameter, flat-bottomed tungsten carbide punch was aligned over a single fiber and was driven at a constant speed of 50 μm/min. The specimen was supported so that the fiber being pushed out can protrude out of the bottom of the sample without any obstruction. A load cell in parallel with the punch constantly monitors the load as the punch is pushed mechanically. Load data were collected at 50-msec intervals by a computer. Conversion of time to actual crosshead displacement allows a load versus displacement curve to be generated as the output of the push-out test. At least ten fibers were pushed out in different regions of the FRC. The push-out apparatus had an upper load limit of 40 N.

3. RESULTS AND DISCUSSION

3.1. Thermogravimetric Analysis

The TGA curves for an SAS monolithic sample hot pressed at 1200°C for 2 h and SCS-6/SAS composite hot pressed at 1450°C for 2 h (V_f = 0.3) recorded at a heating rate of 5°C/min under flowing air from room temperature to 1500°C are given in Fig. 2. The monolithic SAS shows hardly any weight change and appears to be stable over the entire range of temperature in air. In contrast, the SCS-6/SAS composite undergoes a weight loss of ~3.5% due to oxidation of the carbon core and the carbon rich surface coating on the SCS-6 reinforcing fibers.

3.2. Microstructural Analysis

Figure 3 shows micrographs of the polished cross-sections of the unidirectional SCS-6/SAS and SCS-0/SAS composites. On the left is the optical micrograph taken from the plasma etched surface of the SCS-6/SAS composite hot pressed at 1450°C for 2 h under 24 MPa. Plasma etching reveals the composite microstructure of the SCS-6 SiC monofilaments. On the right is an SEM micrograph of the polished cross-section of SCS-0/SAS composite hot pressed at 1400°C for 2 h under 27.6 MPa. Uniform fiber distribution and good matrix flow around the fibers during hot pressing is evident in both composites. Powder XRD patterns of SCS-6/SAS composites hot pressed for 2 h at 1400 or 1500°C and for SCS-0/SAS composite hot pressed at 1400°C for 2 h at 27.6 MPa are shown in Fig. 4 and 5, respectively. β-SiC and monoclinic $SrAl_2Si_2O_8$ are the only phases detected from XRD. This implies that the SAS glass matrix crystallizes primarily to the desired, thermodynamically stable, monoclinic celsian $SrAl_2Si_2O_8$ phase during hot pressing of the composites. Detailed transmission electron micrscopy analysis would be necessary to detect the presence of residual glassy and undesirable crystalline phases.

3.3 Mechanical Properties

Typical stress vs. displacement curves for a hot pressed SAS monolithic and unidirectional CVD SiC_f/SAS composites are shown in Fig. 6. The monolithic SAS, hot pressed at 1200°C for 2 h at 24 MPa, shows a four-point flexural strength of ~130 MPa and fails in a brittle mode as expected. The stress-displacement curve recorded in three-point bend for the SCS-6/SAS composite, hot pressed at 1400°C for 2 h at 24 MPa, having fiber volume of 24% shows graceful failure. It consists of an initial linear elastic region extending up to the first matrix cracking stress, σ_y, of ~289 MPa. Beyond this, there is an extended nonlinear regime of increasing load bearing capacity as most of the reinforcing fibers are still undamaged, intact and carry additional load. The ultimate strength, σ_u, is ~824 MPa. At higher stresses, fiber fracture and pull out occurs, and the load bearing capacity of the composite decreases as fewer and fewer fibers are left intact to carry the load. The SCS-0/SAS composite hot pressed at 1400°C for 2 h under 27.6 MPa also shows graceful failure with σ_y of ~248 MPa and σ_u of only ~285 MPa. However, it shows only limited stressing capability beyond the first matrix cracking stress and low ultimate strength. This is because of the much lower strength of the SCS-0 fibers than that of the SCS-6 fibers. These results clearly demonstrate that reinforcement of the SAS glass-

ceramic with SCS-6 fibers results in a tough and strong composite whereas the SCS-0/SAS composite shows only a very limited improvement in σ_u over the monolithic SAS.

The difficulties in interpretation of the flexure strength results for continuous fiber reinforced composites are recognized. However, the flexure test data are perfectly useful for comparison of the composites made under different hot pressing conditions. Also, when the ratio of the test span length to sample thickness ratio is high enough to minimize shear forces during testing, the value of matrix fracture stress obtained from the flexure test is equivalent to that measured in tension because matrix cracking is the first damage to occur[8] in the composite. The effect of test span length (L), distance between the lower rollers, to sample thickness (d) ratio on the first matrix crack strength and the ultimate strength measured in three-point flexure is shown in Fig. 7 for a SCS-6/SAS composite having a fiber content of 25 volume per cent and hot pressed at 1350 °C for two hours under 24 MPa pressure. Initially both σ_y and σ_u increase sharply with increase in L/d ratio but seem to level off at L/d > ~25. At high L/d ratios, the sample failure occurred on the tensile surface where the tensile stresses are the highest, whereas delamination was observed at low L/d ratios. All further flexure measurements were carried out using an L/d ratio of greater than 25.

The effect of hot pressing temperature on room temperature flexural strength of the unidirectional SCS-6/SAS composites is shown in Fig. 8. Also shown are the results for the monolithic SAS glass-ceramic hot pressed at 1200 °C. The monolithic SAS shows a flexural strength of ~130 MPa. Values of both the first matrix cracking stress and the ultimate strength for the composites, having a fiber content of ~25 volume %, do not show much change with hot pressing temperature. The strength data for the composites shown here and in subsequent figures are the average values for at least five test specimens. The effect of hot pressing time on room temperature flexural strength of unidirectional SCS-6 fiber-reinforced SAS composites hot pressed at 1450 °C under 24 MPa is shown in Fig. 9. The fiber content was ~24 volume %. The first matrix cracking stress hardly shows any change, but the ultimate strength increases with time of hot pressing. The two-hour hot pressed FRC shows the highest ultimate strength.

The influence of hot pressing pressure on room temperature flexural strength of unidirectional

SCS-6/SAS composite hot pressed for 2 h at 1450°C or 1250 °C is shown in Fig. 10 and 11, respectively. The fiber loading was ~ 26 and ~ 22 volume %, respectively. Values of first matrix cracking stress and ultimate strength increased with pressure of hot pressing at both temperatures. Composites hot pressed under 27.6 MPa (4 KSI) pressure exhibited the highest first matrix cracking and ultimate strengths. The increase is strength with hot pressing pressure is probably due to increase in the densities of the composites as shown in Fig. 12.

Typical room temperature physical and mechanical properties of a unidirectional SCS-0/SAS composite having fiber volume fraction of 24 % and hot pressed at 1400°C for 2 h under 27.6 MPa are shown in Table I. The composite had a density of 2.99 g/cm^3 which is ~98% of the theoretical value. The elastic modulus was 102 ± 10 GPa measured from three point bend test. Typical values of first matrix cracking stress and ultimate strength were ~ 231 ± 20 MPa and 265 ± 17 MPa, respectively. The first matrix cracking strain was ~0.22%.

Effects of fiber content on various mechanical properties, measured in 3-point flexure, of SCS-6/SAS composites hot pressed at 1400°C for 2 h under 27.6 MPa pressure are listed in Table II. Variations in first matrix cracking stress and ultimate strength with the fiber content are shown in Figure 13. Values of both σ_y and σ_u increased with the fiber content, reached a maximum at V_f = ~0.35 and dropped with further increase in V_f. For hot pressed ceramic grade Nicalon reinforced pyrex glass composites, Dawson *et al.*[37] found that composite strength increased linearly with fiber volume fraction from 0.2 to 0.6. Hegeler *et al.*[38] reported that for Nicalon/glass composites made by hot pressing, the composite strength increased with fiber content, reaching a maximum at V_f = 0.5 and then dropped rapidly for higher V_f. For hot pressed Si_3N_4 matrix reinforced with CVD SiC (SCS-2) monofilaments, Shetty *et al.*[39] found that the composite strength was virtually independent of the fiber volume fraction from V_f ~ 0.05 to 0.45. However, recently Xu *et al.*[40] found that for hot pressed Si_3N_4 matrix reinforced with CVD SiC (SCS-6) fibers, the composite strength increased with fiber volume fraction from 0.14 to 0.29. However, when the fiber content was raised to 55%, the composite strength dropped due to degradation in fiber strength as a result of damage of fibers from contact with surrounding fibers and abrasive matrix particles during hot pressing.

Figure 14 compares the measured values of the elastic modulus of the SCS-6/SAS composite

with those calculated from the rule-of-mixtures using the relationship

$$E_c = V_m E_m + V_f E_f \quad (2)$$

where E is the elastic modulus, V is the volume fraction and the subscripts c, m, and f refer to the composite, matrix, and fiber, respectively. Values of 70 GPa and 400 GPa were used for the elastic modulii of the SAS matrix and the SCS-6 fibers, respectively, for the calculations. The solid line represents the results obtained from equation (2). The measured E_c values are in agreement with those expected from the simple rule-of-mixtures.

SEM micrographs of fracture surfaces, after the 3-point bend test, of unidirectional SCS-6/SAS and SCS-0/SAS composites hot pressed at 1400°C for 2 h under 27.6 MPa are shown in Fig. 15. Long lengths of fiber pull out are observed for the SCS-6/SAS composite, indicating a weak fiber/matrix interface and a tough composite. In contrast, only limited and short lengths of fiber pull out are seen in the SCS-0/SAS composite which would result in only limited toughening behavior. Some of the fibers do not show any pull out indicating strong bonding with the matrix. The surface of the pulled out fibers is clean and smooth indicating no chemical reaction between the SCS-6 or SCS-0 fibers and the SAS matrix during hot pressing at high temperature. These results are consistent with the stress-strain behavior observed for these FRCs.

3.4. Fiber/Matrix Interface

SEM micrographs showing magnified views of the fiber/matrix interface in the unidirectional SCS-6/SAS and SCS-0/SAS composites hot pressed at 1400°C for 2 h under 27.6 MPa are given in Fig. 16. The interface is clean and the carbon rich double coating on the SCS-6 fiber surface is unaffected. This again indicates no chemical interaction between the fiber and the matrix during high temperature composite processing.

In order to achieve high strength and, in particular, high toughness in the fiber-reinforced ceramic matrix composites, the fiber/matrix interfacial shear strength must be tailored such that

the bond is strong enough to allow transfer of load from the matrix to the fibers, but weak enough so that an advancing matrix microcrack can be deflected at the interface by fiber/matrix debonding. To evaluate the fiber-matrix interfacial shear strengths (ISS), fiber push out tests were carried out. Typical fiber push out load vs. crosshead displacement curves for SCS-6/SAS glass-ceramic matrix composite hot pressed at 1400 °C for 2 h under 27.6 MPa are presented in Fig. 17 for specimens of two different thicknesses. Similar load-displacement curves for the fiber push out in SCS-0/SAS composite hot pressed at 1400°C for 2 h under 27.6 MPa are shown in Fig. 18 for a 1.44 mm thick sample. The initial linear region corresponds to the elastic response of the material. The peak load, P_{debond} corresponds to the fiber/matrix debonding load and the sudden drop in load represents debonding of the fiber. Following debonding, the slight increase in load corresponds to additional debonding. At the maximum load, the entire length of the fiber has debonded and the fiber begins to exit from the opposite face of the composite. The decrease in load is due to the decrease in embedded length of the fiber. The steady state load represents the sliding friction at the interface. A plot of fiber/matrix debonding load vs. sample thickness for the SCS-6/SAS composite is given in Fig. 19. The fiber debonding load varies linearly with the thickness of the sample used for fiber push out tests.

Values of the ISS for debond (τ_{debond}) and frictional sliding stress ($\tau_{friction}$) were calculated from

$$\tau = P/(2\pi r_f L_f) \tag{3}$$

where τ is the interfacial shear strength, r_f is the radius of the fiber, L_f is the length of the embedded fiber, and P is the load corresponding to debond or friction. This equation assumes a uniform interfacial shear stress along the length of the fiber/matrix interface. Values of τ_{debond} and $\tau_{friction}$ evaluated from fiber push out tests for the SCS-6/SAS and SCS-0/SAS composites are listed in Table III. For the SCS-6/SAS composites, τ_{debond} and $\tau_{friction}$ increased systematically (Table IV) as the time of hot pressing was increased from 15 min. to 2 h at 1450°C under 24 MPa. Values shown are the mean values for 8-10 push out tests. For the SCS-6/SAS composite, samples of four different thicknesses were tested and the values are in good agreement. For the SCS-0/SAS composite, the mean values of τ_{debond} and $\tau_{friction}$ were determined to be $\sim 17.5 \pm 2.7$ MPa and 11 .3 $\pm$ 1.6 MPa, respectively. One fiber even gave a value of 56 MPa for τ_{debond}.

Some fibers did not debond even at an applied load of 40 N, the upper limit of the test apparatus, resulting in $\tau_{debond} > 62$ MPa. Values of τ_{debond} and $\tau_{friction}$ are seen to be much higher for the SCS-0/SAS composite than for the SCS-6/SAS system. These results indicate that some of the fibers in the SCS-0/SAS composite are strongly bonded with the matrix. This is consistent with the stress-strain curves and the extent of fiber pullout for these composites as seen earlier in the SEM micrographs of the fracture surfaces. The fibers which did not show any pull out are the ones strongly bonded. In an earlier study by the present author[29], no chemical reaction was observed between the SCS-0 fiber and $BaO.Al_2O_3.2SiO_2$ (BAS) matrix in the composite hot pressed at 1400°C for 2 h under 24 MPa. Examination of the fracture surface revealed fiber/matrix debonding at the interface, fiber pull-out, and crack deflection around the fibers indicating a weak fiber/matrix interface and a tough composite. In contrast, Murthy and Lewis[30] reported the formation of a carbon-rich layer at the fiber/matrix interface in SiC (Nicalon or Tyranno) fiber-reinforced non-stoichiometric BAS composite hot pressed at 1350°C. The reaction layer was an admixture of microcrystalline graphite, silica, and barium. Extensive diffusion of barium well into the fiber was also observed. However, the SiC whisker/BAS glass interface was found to be nonreactive.

The values of ~ 6.5 MPa for τ_{debond} and ~ 4.2 MPa for $\tau_{friction}$ obtained in the present study for the SCS-6/SAS composite are comparable to those reported for other SiC fiber-reinforced glass-ceramic matrix composites. In the Nicalon fiber reinforced CAS glass-ceramic matrix composites, the value of $\tau_{friction}$ was evaluated[10] to be 5 MPa using the Aveston, Cooper, and Kelly (ACK) model[13] from the matrix crack spacings measured at room temperature. This is in fairly good agreement with the values of 3-5 MPa obtained from the micro-indentation method. In the same composite system, Wang and Parvizi-Majidi[14] obtained a value of 14.4 ± 3.2 MPa for $\tau_{friction}$ using the matrix crack spacing ACK model and values ranging from 12.4 ± 2.6 MPa to 17.7 ± 2.0 MPa from fiber push-out and fiber push-in tests, respectively. Evans[15] reported a value of 9 MPa for $\tau_{friction}$ in a Nicalon/CAS composite, compared with a value of only 2 MPa for the Nicalon fiber-reinforced LAS glass-ceramic matrix composite from similar calculations. For the SCS-6 fiber-reinforced MAS (Cordierite) matrix composite, values of τ_{debond} and $\tau_{friction}$ have been reported[16] to be 11 MPa and 5 MPa, respectively. Values of ISS for various oxide and nonoxide ceramic matrix composites reinforced with Nicalon or SCS-6 fibers have been

summarized by Weihs *et al* [17]. Very low values of τ_{debond} (~0.5 - 1.5 MPa) and $\tau_{friction}$ (~0.15 - 1.23 MPa) have been obtained[18] in the SCS-6 fiber reinforced $NaZr_2P_3O_{12}$ matrix composite from single fiber push-out test.

From fiber pushout and pullout tests, the fiber/matrix interfacial shear strengths have been evaluated[21] to be 15.6 ± 8.3 MPa for the SCS-0/borosilicate glass and 3.9 ± 1.4 MPa for the SCS-6/borosilicate (CGW #7761) glass matrix composites. Some chemical reaction between the uncoated SCS-0 fiber and the glass was observed[21] after composite processing whereas no reaction was observed between the glass and the SCS-6 fiber having carbon rich surface coatings. Goettler and Faber[22] measured the fiber/matrix interfacial shear properties of SiC fibers in sodium borosilicate glass matrix system using single fiber pullout tests. A carbon coating on the SiC fiber surface was an effective reaction barrier in preventing the fiber/matrix bonding and oxidation of the fibers by the glass matrix. However, coatings having higher carbon content resulted in stronger bonding at the interface.

The presence of residual stresses in the composite can have significant influence on the fiber/matrix interfacial shear strength. These residual stresses can arise from various sources, but mainly come from thermal expansion mismatch between the fiber and the matrix. When the thermal expansion of the fiber is smaller than that of the matrix ($\alpha_f < \alpha_m$), the matrix will shrink more than the fibers upon cooling the FRC from the processing temperature. The matrix will radially compress the fibers, increasing friction at the fiber/matrix interface. However, when $\alpha_f > \alpha_m$, as in the composite system of the present study, the fiber-matrix interfacial region is under tension in the FRC composite upon cooling from the processing temperature. If there is poor bonding at the interface, this may result in fiber separation from the matrix, as suggested by the similar values for τ_{debond} and $\tau_{friction}$ for the SCS6/SAS composites in the present study. In any case, a low interfacial shear strength typically results in a fibrous failure mode and a tough composite which, indeed, is the case for the SCS-6/SAS composite of the present study. However, in the SCS-0/SAS composites, some of the fibers are more strongly bonded to the matrix as indicated by the values of τ_{debond} which should result in only limited short length of fiber pull-out as observed, and a not-so-tough composite. Similar values of τ_{debond} and $\tau_{friction}$ indicate that the fiber/matrix interface in SCS-6/SAS composites is frictionally coupled, i.e., the

the interfacial bonding between the fiber and the matrix is negligible. The higher values of τ in SCS-0/SAS composites may be attributed to fiber/matrix interlocking due to a rough surface of the uncoated fiber.

SEM micrographs showing in-place and pushed out fibers in SCS-6/SAS and SCS-0/SAS composites are shown in Fig. 20. The surfaces of the pushed out fibers appear to be smooth. The carbon-rich double coating on the SCS-6 fiber is still intact. Debonding occurs between the matrix and the outer carbon rich coating on the SCS-6 fiber surface. Also, there appears to be no chemical interaction or interdiffusion between SCS-6 fiber and the matrix during high temperature composite processing. Particles on fiber surfaces and the matrix are believed to be debris from sample preparation. An SEM micrograph and the x-ray maps of various constituent elements in the fiber-matrix interface region taken from the polished cross-section of a unidirectional SCS-0/SAS composite hot pressed at 1400°C for 2 h at 27.6 MPa are presented in Fig. 21. On this scale, there appears to be no interdiffusion of the elements between the fiber and the matrix after high temperature processing of the composite. In an earlier study by the present author[29], no chemical reaction was observed between the SCS-0 fiber and the BAS matrix in a composite hot pressed at 1400°C for 2 h at 24 MPa.

3.5. Comparison with Micromechanical Models

It is also interesting to compare the measured values of first matrix cracking stress and ultimate bend strength with those predicted from the theoretical models. Two different types of approaches, based on either fracture mechanics or energy balance, have been applied to the problem of matrix cracking in composites for the matrix failure strain and the stress to propagate a crack.

Using fracture mechanics analysis, Marshall, Cox, and Evans[23] have modelled matrix cracking in brittle matrix fiber-reinforced composites by taking into account the crack closure effects of the frictionally bonded bridging fibers. For large cracks, the matrix cracking stress is independent of the crack size and a steady state matrix cracking stress, σ_y, is given by[23]:

$$\sigma_y = 1.817[(1 - \nu^2)\, K_{IC}^2\, \tau_{friction}\, E_f\, V_f^2\, V_m\, (1 + E_f V_f / E_m V_m)^2 / (E_m\, r_f)]^{1/3} \qquad (4)$$

where ν is the composite Poisson's ratio, K_{IC} the matrix fracture toughness, $\tau_{friction}$ the sliding frictional stress at the interface, V_f the fiber volume fraction, V_m the matrix volume fraction, r_f the fiber radius, E_f the fiber elastic modulus, and E_m the matrix elastic modulus. Using the following values of the various parameters: $\nu = 0.2$, $K_{IC} = 1$ MPa.m^{½}, $E_f = 390$ GPa, $E_m = 69$ GPa, $V_m = 0.76$, $r_f = 71$ μm, and $V_f = 0.31$, $\tau_{friction} = 4.2$ MPa for the SCS-6/SAS composite and $V_f = 0.24$, $\tau_{friction} = 11.3 \pm 1.6$ MPa for the SCS-0/SAS composite, the values of σ_y predicted from equation (4) are 117 MPa and 121 MPa, respectively for the two composites. These values are low in comparison with the measured 3-point bend strengths of 290 $\pm$ 40 MPa and 231 $\pm$ 20 MPa, respectively. However, it may be pointed out that eq. (4) estimates the lower bound σ_y at large crack lengths above the transition crack length, $C_m/3$, given by the following equation[23]:

$$C_m = (\pi/4I^{4/3}) [K_{IC} E_m V_m^2 r_f (1 + E_f V_f/E_m V_m)/\tau_{friction} V_f^2 E_f (1 - \nu^2)]^{2/3} \quad (5)$$

where I is a crack geometry constant with a value of 1.2 for straight cracks and 2/3 for penny cracks. An important feature of Marshall *et al.*'s theory is its prediction of a flaw size dependence of matrix microcracking stress for flaw sizes smaller than the critical size. The matrix cracking stress approaches the steady state value for cracks of lengths $\geq C_m/3$. In contrast, for cracks shorter than $C_m/3$, σ_y should show a marked dependence on crack size and significant departure from the steady-state value. Using the above values for various parameters, the values of C_m calculated for the SCS-6/SAS and SCS-0/SAS composite systems from eq. (5) were 886 μm and 625 μm, respectively. C_m values of 313 μm, 68 μm, 660 μm, and 3.5 mm have been reported for the Nicalon/lithium aluminosilicate glass-ceramic[23], carbon/glass[23], SiC(SCS-6)/zircon[24], and SiC(SCS-6)/sodium zirconium phosphate (NZP)[18] composites, respectively. This implies that $C_m/3$ is several fiber spacings for all of these composite systems indicating the existence of a steady-state condition. Since the inherent flaws in ceramic materials are usually of microstructural dimensions, these results indicate[23] that the matrix cracking stress for these composites is not considerably reduced by further introduction of larger flaws during composite fabrication, machining or service or by the extension of pre-existing flaws in thermal shock or environmentally assisted slow crack growth.

The above eq. (5) taken from the work of Marshall *et al.*[23] appears to be in error. Using equations (23a) and (17b) from ref. 23, the following expression is obtained for C_m

$$C_m = (\pi/4I^{4/3}) [(K_{IC} r_f E_m V_m)/(\tau_{friction} V_f^2 E_f (1-\nu^2))]^{2/3} \quad (6)$$

rather than eq. (5) above. From eq. (6), values of 487 μm and 379 μm are obtained for C_m for the SCS-6/SAS and SCS-0/SAS composites, respectively. Since the $C_m/3$ value for the SCS-0/SAS composites of the present study is smaller than the filament diameters, it would indicate departure from the steady-state matrix cracking stress and dependence on the crack size. On the other hand, a steady-state condition would be expected to exist for the SCS-6/SAS composites. These predictions of the micromechanical models need to be verified from experimental data.

By using a simple energy balance approach, similar to that of Griffith in determining the stress necessary to propagate cracks in brittle solids, the following equation[13,25] has been derived for the matrix cracking stress in a composite consisting of a low failure strain matrix reinforced with high failure strain continuous fibers:

$$\sigma_y = [(12\tau_{friction} \Gamma_m V_f^2 E_f E_c^2)/\{r_f(1-V_f)E_m^2\}]^{1/3} \quad (7)$$

where Γ_m is the matrix fracture surface energy, $E_c = V_fE_f + V_mE_m$, and other terms have the same meaning as above. It is apparent from this equation that the first matrix cracking stress can be enhanced by increasing fiber-matrix interfacial sliding stress, by using fibers of smaller radius, and by increasing the volume fraction of fibers. It might also be increased, less easily, by increasing the ratio E_f/E_m. The matrix microcracking may also be suppressed by placing the matrix in compression through choosing $\alpha_f > \alpha_m$, although for isotropic fibers this will result in contraction of the fibers away from the matrix and a potential decrease in fiber-matrix shear strength. It is important to optimize the fiber-matrix bond strength carefully as too strong a bond will result in a brittle composite with low toughness. Typical values of Γ_m for ceramics range from 20 to 40 J/m^2 as quoted by Briggs and Davidge.[34] Values of Γ_m for calcium aluminosilicate and lithium aluminosilicate glass-ceramic matrices have been reported to be 25 and 20-30 J/m^2, respectively. Taking $\Gamma_m \approx 25$ J/m^2 for the SAS glass ceramic matrix, and values of other

parameters as shown above, the σ_y for the SCS-6/SAS and SCS-0/SAS composites were calculated from eq. (7) to be 179 MPa and 185 MPa, respectively, without any corrections for the expected residual stresses in the matrix. In spite of higher fiber volume fraction in SCS-6/SAS composite, the calculated σ_y is higher for the SCS-0/SAS composite. This is because of much higher value of sliding frictional stress at the interface, $\tau_{friction}$, for the SCS-0/SAS composite which, according to eq. (7), should result in higher σ_y. These calculated values of σ_y are close to those obtained from eq. (4) but much lower than the values of 290 $\pm$ 40 MPa and 231 $\pm$ 20 MPa measured in 3-point flexure for the two composites, respectively. However, it may be pointed out that generally the tensile strengths are lower than those measured in bending and the tensile test results, rather than the flexural data, are more meaningful for comparison with the predictions of the micromechanical models. Also, the effects of internal residual stresses arising from the thermal expansion mismatch between the fiber and the matrix, which have been neglected in the calculations of the above models, must be taken into account.

The axial residual stress in the matrix, σ_m, in the composite as a result of cooling from the hot pressing temperature is given by[26]

$$\sigma_m = [E_f V_f (\alpha_f - \alpha_m) \Delta T]/[1 + V_f(E_f/E_m - 1)] = [E_f V_f (\alpha_f - \alpha_m) \Delta T] [E_m/E_c] \quad (8)$$

where α_m and α_f are the thermal expansion coefficients of the matrix and the fibers, respectively, ΔT is the temperature range over which the composite has been cooled after processing, and the other terms are the same as described above. For composites of the present study hot pressed at 1400°C and using values of various parameters as $\alpha_f = 4.4 \times 10^{-6}/°C$, $\alpha_m = 2.5 \times 10^{-6}/°C$, $E_f = 390$ GPa, and $E_m = 69$ GPa, values of the axial residual stress, σ_m, in the matrix at room temperature are calculated from eq.(8) to be +129 MPa for SCS-6/SAS ($V_f = 0.31$) and +115 MPa for SCS-0/SAS ($V_f = 0.24$) composites, respectively. The positive σ_m implies that the SAS glass-ceramic matrix will be in compression as fibers try to shrink more than the matrix and the residual stresses will be beneficial tending to close the incipient matrix cracks. As mentioned earlier, the residual stresses present in the as-manufactured composite are not considered in the derivation of eq. (4) or (7). Thermal residual stress present in the composite, $\Delta\sigma_c$, is given by the expression

$$\Delta\sigma_c = \sigma_m \cdot (E_c/E_m) = E_f V_f (\alpha_f - \alpha_m) \Delta T \quad (9)$$

For SCS-6/SAS and SCS-0/SAS composites of the present study hot pressed at 1400°C, values of $\Delta\sigma_c$ at room temperature are calculated from eq. (9) to be +315 MPa and +244 MPa, respectively. To account for the residual stress effects in the composite due to fiber-matrix thermal expansion mismatch, the stress calculated from eq. (9) should be added to those determined from eq. (4) or (7). This results in calculated σ_y values between 432 and 494 MPa for the SCS-6/SAS and between 365 and 429 MPa for the SCS-0/SAS composites which are much higher than the experimentally measured three-point flexural strengths of 290 ± 40 MPa and 231 ± 20 MPa, respectively. Also, the tensile test results, rather than the flexural data, are more meaningful for comparison with the predictions from the micromechanical models and generally the tensile strengths are lower than the flexural strengths. This would result in greater discrepancy between the calculated and the measured tensile strength data. Hence, the current micromechanical models do not appear to be useful in predicting the first matrix crack stress for the large diameter fiber-reinforced composites of the present study.

An analytical estimate of the ultimate tensile strength of a fiber-reinforced composite is given by the equation[27,33]:

$$\sigma_u = V_f \sigma_f [\{1/(m+2)\}^{1/(m+1)} \{(m+1)/(m+2)\}] [2\tau_{friction} L_o/(\ln 2)\sigma_f r_f]^{1/m+1} \quad (10)$$

where V_f is volume fraction of fibers in the loading direction, r_f is the fiber radius, σ_f is the mean fiber tensile strength at a gauge length of L_o, m is the Weibull modulus, and $\tau_{friction}$ is the frictional sliding stress at the fiber-matrix interface. Equation (10) takes into account the proper gauge length of fibers relevant to composite tensile failure as well as the fiber bundle failure in brittle matrix composites. In eq. (10), the first two terms, $V_f\sigma_f$, give the rule-of-mixtures strength of the composite using the mean fiber strength at the test gauge length L_o. The third term within brackets is the statistical bundle-like factor depending only on m. This factor describes the tendency of the statistically weaker fibers to control the composite failure and the counteracting fact that broken fibers still have substantial load-carrying capability due to the sliding resistance $\tau_{friction}$. Thus, the first three terms together essentially give the bundle rule-of-

mixtures strength of the FRC. The last term, called the composite factor, in eq. (10) accounts for the change in fiber strength from gauge length L_o to the characteristic gauge length relevant to composite tensile failure and for the load carried by the broken fibers in brittle matrix composites. The composite factor is critical for predicting an accurate value of σ_u for the composite. Tensile strengths of SCS-6 fibers have been recently measured by various researchers[28, 31,32]. Taking values of σ_f = 4170 MPa, m = 5.2, L_o = 4 cm, r_f = 71 μm for the SCS-6 fibers from a recent study[31], and $\tau_{friction}$ = 4.2 MPa, V_f = 0.31 for the SCS-6/SAS composite, a value of σ_u = 877 MPa was calculated from eq. (10). The calculated value of σ_u is much higher than the measured 3-point flexure strength of 625 $\pm$ 50 MPa. This is particularly true considering that the ultimate strengths of composites measured in flexure are reported[9,10] to be always higher than those measured in tension, by a factor of between 1.5 and 2.5 depending on lay-up. This is generally ascribed to the differences in stress distributions in the test specimens during flexure and tensile tests. During tensile testing, the entire gauge section is under tensile loading, but only a part of the sample is under tension during flexure test. Thus, the flexure strength data are not very useful for comparison with the predictions of the micromechanical models which are based on the assumptions of uniaxial tensile loading.

Another reason for the discrepancy between the measured and predicted values of σ_u could be the fiber strength degradation occuring during composite fabrication. Strength of fibers after high temperature composite processing should be used in eq. (10). However, strength of the *in situ* fibers in the FRC following hot pressing is unknown unless fibers can be extracted from the composite without further damage to the fibers and tensile tested. The etchants used to dissolve away the celsian matrix from the SiC_f/SAS composite would invariably damage the fiber surface. Abrasive damage to the fiber surface during composite processing may also affect the fiber strength. Also, the interactions occurring during high temperature composite processing are known to reduce the fiber strength. For example, the strength of Nicalon fibers is 3 GPa, but the strength of the fibers extracted from Nicalon/Pyrex composites following processing at $\sim$950°C is reduced by $\sim$50%.[11] The degradation in the fiber strength depends on the temperature and pressure used during processing as well as on the reactivity between the fiber and the matrix. The room temperature strength of SCS-0 fibers degrades[12] after exposure to temperatures beyond $\sim$1200°C in argon, due to recrystallization and grain growth of the SiC

grains in the outer zone of the fibers. Strength degradation of the fibers increased with temperature and time of exposure at temperatures above 1200°C. For example, the room temperature flexural strength of SCS-0 fibers degraded from 3.2 GPa to 2.5 GPa and to 1.9 GPa after 1h exposure in 0.1 MPa argon pressure at 1400°C and 1600°C, respectively. In contrast, the room temperature strength of the SCS-6 fibers remained unchanged at ~5.5 GPa after 1 h exposure in 0.1 MPa argon pressure at 1400°C, but its strength did degrade[12] after heat treatments at higher temperatures. This partly explains the low strengths observed for the SCS-0/SAS composite hot pressed at 1400°C for two hours, and the much higher strengths of the SCS-6/SAS composites in the present study.

4. SUMMARY OF RESULTS

Unidirectional CVD SiC fiber-reinforced SAS glass-ceramic matrix composites have been fabricated by hot pressing under various temperature, pressure, and time. Three point flexure test of composites should be carried out using a test span to thickness ratio of ~25 or greater in order to avoid sample delamination. Unidirectional SCS-6/SAS composites having a first matrix cracking stress of ~300 MPa and an ultimate bend strength of 825 MPa have been fabricated. Uncoated CVD SiC_f(SCS-0)/SAS composites were not as strong and showed only limited improvement over SAS monolithic. No chemical reaction between the SCS-6 fibers and the SAS matrix was observed after high temperature processing. From fiber push-out tests, the fiber/matrix ISS (τ_{debond}) was found to be ~6.7 ± 2.3 MPa for SCS-6/SAS composites indicating a weak interface. However, for the uncoated SCS-0 fiber reinforced SAS composite, a much higher value of τ_{debond} (~17.5 ± 2.7 MPa) was observed; some of the fibers were so strongly bonded that they could not be pushed out. Predicted values of first matrix cracking stress and ultimate strength using various micromechanical models have been compared with those measured experimentally.

5. CONCLUSIONS

It may be concluded that strong, tough, and almost fully dense unidirectional CVD SiC_f(SCS-6) fiber-reinforced SAS glass-ceramic matrix composites can be obtained by hot pressing at

~1250 - 1400 °C for 2 h at 20 - 27 MPa (3 - 4 KSI). Also, uncoated SCS-0 fiber is not appropriate for the reinforcement of the SAS glass-ceramic matrix. CVD SiC SCS-6 fibers and the SAS matrix are chemically compatible even at temperatures as high as 1400°C. The current theoretical models do not appear to be appropriate in predicting the matrix microcracking stress or the ultimate strength of the large diameter CVD SiC fiber reinforced SAS glass-ceramic matrix composites.

ACKNOWLEDGMENTS: Thanks are due to John Setlock, Dan Gorican and Richard First for their assistance in composite processing and testing.

REFERENCES

1. Bansal, N.P., Ceramic Fiber Reinforced Glass-Ceramic Matrix Composite, U. S. Patent 5,214,004, May 25, 1993.

2. Bansal, N.P., Method of Producing a Ceramic Fiber-Reinforced Glass-Ceramic Matrix Composite, U. S. Patent, 5,281,559, January 25, 1994.

3. Bansal, N.P., SiC/Celsian Glass-Ceramic Matrix Composites, HITEMP Review 1991: Advanced High Temperature Engine Materials Technology Program, NASA CP-10082, 1991, pp. 75-1 to 75-15.

4. Wawner, F.W., Teng, A.Y., and Nutt, S.R., Microstructural Characterization of SiC (SCS) Filaments, *SAMPE Quart.*, **14**[3] 39-45 (1983).

5. Eldridge, J.I., Bhatt, R.T., and Kiser, J.D., Investigation of Interfacial Shear Strength in SiC/Si_3N_4 Composites, NASA TM-103739, 1991.

6. Bansal, N.P., and Drummond, C.H., III, Kinetics of Hexacelsian-to-Celsian Phase Transformation in $SrAl_2Si_2O_8$, *J. Am. Ceram. Soc.*, **76**[5] 1321-1324 (1993)

7. Bansal, N.P., Fiber-Reinforced Refractory Glass-Ceramic Composites, in HITEMP Review 1993: Advanced High Temperature Engine Materials Technology Program. Vol. III Turbine Materials-- CMCs, Fibers, NASA CP 19117, p. 63-1 to 63-13 (1993).

8. Marshall, D.B., and Evans, A.G., Failure Mechanisms in Ceramic-Fiber/Ceramic Matrix Composites, in *"Ceramic Containing Systems"*, A.G.Evans, Ed., Noyes Publications, Park Ridge, NJ, 1986, pp. 90-123.

9. Singh, R.N., Influence of Testing Method on Mechanical Properties of Ceramic Matrix Composites, *J. Mater. Sci.*, **26**[23] 6341-6351(1991).

10. Bleay, S.M., Scott, V.D., Harris, B., Cooke, R.G. and Habib, F.A., Interface Characteriza--tion and Fracture of Calcium Aluminosilicate Glass-Ceramic Reinforced with Nicalon Fibers, *J. Mater. Sci.*, **27**[10] 2811-2822 (1992).

11. Prewo, K.M., Tension and Flexural Strength of Silicon Carbide Fiber Reinforced Glass Ceramics, *J. Mater. Sci.*, **21**[10], 3590-3600 (1986).

12. Bhatt, R.T., and Hull, D.R., Microstructural and Strength Stability of CVD SiC Fibers in Argon Environment, NASA TM 103772, 1991.

13. Aveston, J., Cooper, G.A., and Kelly, A., Single and Multiple Fracture, in *"The Properties of Fiber Composites"*, IPC Sci. and Technol. Press, Guildford, 1971, pp. 15-26.

14. Wang, S.-W., and Parvizi-Majidi, A., Mechanical Behavior of Nicalon Fiber-Reinforced Calcium Aluminosilicate Matrix Composites, *Ceram. Eng. Sci. Proc.*, **11**[9-10] 1607-1616

(1990).

15. Evans, A.G., The Mechanical Performance of Fiber-Reinforced Ceramic Matrix Composites, in *"Mechanical and Physical Behavior of Fiber-Reinforced Ceramic Matrix Composites"*, edited by S.I. Andersen, H. Lilholt, and O.B. Pedersen, Riso, Denmark, 1988, pp. 13-34.

16. Dharani, L.R., Rahaman, M.N., and Wang, S.-H., Interfacial Shear Stress in SiC Fiber Reinforced Cordierite, *J. Mater. Sci.*, **26**[3] 655-660 (1991).

17. Weihs, T.P., and Nix, W.D., Experimental Examination of the Push-Down Technique for Measuring the Sliding Resistance of Silicon Carbide Fibers in a Ceramic Matrix, *J. Am. Ceram. Soc.*, **74**[3] 524-534 (1991).

18. Griffin, C.W., Limaye, S.Y., Richerson, D.W., and Shetty, D.K., Correlation of Interfacial and Bulk Properties of SiC-Monofilament Reinforced Sodium Zirconium Phosphate Composites, *Ceram. Eng. Sci. Proc.*, **11**[9-10], 1577-1591(1990).

19. Bright, J., Shetty, D.K., Griffin, C.W., and Limaye, S.Y., Interfacial Bonding and Friction in Silicon Carbide (Filament)-Reinforced Ceramic- and Glass-Matrix Composites, *J. Am. Ceram. Soc.*, **72**[10] 1891-1898 (1989).

20. Shetty, D.K., Shear-Lag Analysis of Fiber Push-Out (Indentation) Tests for Estimating Interfacial Frictional Stress in Ceramic Matrix Composites, *J. Am. Ceram. Soc.*, **71**[2] C107-C109 (1988).

21. Jurewicz, A.J.G., Kerans, R.J., and Wright, J., The Interfacial Strengths of Coated and Uncoated SiC Monofilaments Embedded in Borosilicate Glass, *Ceram. Eng. Sci. Proc.*, **10**[7-8], 925-937 (1989).

22. Goettler, R.W., and Faber, K.T., Interfacial Shear Stresses in Fiber-Reinforced Glasses, *Composites Sci. Technol.*, **37**[1-3] 129-147 (1989).

23. Marshall, D.B., Cox, B.N., and Evans, A.G., The Mechanics of Matrix Cracking in Brittle Matrix Fiber Composites, *Acta Metall.*, **33**[11] 2013-2021(1985).

24. Singh, R.N., Influence of Interfacial Shear Stress on First-Matrix Cracking Stress in Ceramic Matrix Composites, *J. Am. Ceram. Soc.*, **73**[10] 2930-2937 (1990).

25. Budiansky, B., Hutchinson, J.W., and Evans, A.G., Matrix Fracture in Fiber-Reinforced Ceramics, *J. Mech. Phys. Solids*, **34**[2] 167-189 (1986).

26. Phillips, D.C., Sambell, R.A.J., and Bowen, D.H., The Mechanical Properties of Carbon Fiber Reinforced Pyrex Glass, *J. Mater. Sci.*, **7**, 1454-1464 (1972).

27. Curtin, W.A., Theory of Mechanical Properties of Ceramic-Matrix Composites, *J. Am. Ceram. Soc.*, **74**[11] 2837-45 (1991).

28. Draper, S.L., Brindley, P.K., and Nathal, M.V., Effect of Fiber Strength on the Room Temperature Tensile Properties of SiC/Ti-24Al-11Nb, *Metall. Trans. A*, **23A**, 2541-48 (1992).

29. Bansal, N.P., Processing and Properties of CVD SiC Fiber-Reinforced $BaAl_2Si_2O_8$ Glass-Ceramic Matrix Composites, in Proc. of 17th Conference on Metal Matrix, Carbon, and Ceramic Matrix Composites, Cocoa Beach, FL, Jan. 10-15, 1993; NASA CP 3235, Part 2, pp 773 - 797 (1994).

30. Murthy, V.S.R., and Lewis, M.H., Matrix Crystallization and Interface Structure in SiC-Celsian Composites, *Br. Ceram. Trans. J.*, **89**[5] 173-174 (1990).

31. Martineau, P., Lahaye, M., Pailler, R., Naslain, R., Couzi, M., and Cruege, F., SiC Filament/Titanium Matrix Composites Regarded as Model Composites. Part 1. Filament Microanalysis and strength Characterization, *J. Mater. Sci.*, **19**[8] 2731-48 (1984).

32. MacKay, R.A., Draper, S.L., Ritter, A.M., and Siemers, P.A., A Comparison of the Mechanical Properties and microstructures of Intermetallic Composites Fabricated by Two Different Methods, *Metall. Trans. A*, **25A**[7] 1443-1455 (1994).

33. Curtin, W.A., Ultimate Strengths of Fiber-Reinforced Ceramics and Metals, *Composites*, **24**[2] 98-102 (1993).

34. Briggs, A. and Davidge, R.W., Borosilicate Glass Reinforced with Continuous Silicon Carbide Fibers: A New Engineering Ceramics, *Mater. Sci. Eng.*, **A109**, 363-372 (1989).

35. Bansal, N.P., Strontium Aluminosilicate Glass-Ceramic Composites Reinforced With Uncoated CVD SiC Fibers, NASA TM 106672 (1994).

36. Bansal, N. P., McCluskey, P., Linsey, G., Murphy, D., and Levan, G., Processing and Properties of Nicalon-Reinforced Barium Aluminosilicate (BAS) Glass-Ceramic Composites, Paper Presented at 19th Annual Conference on Composites, Materials, and Structures (Restricted Sessions), Cocoa Beach, FL; January 9-10, 1995.

37. Dawson, D. M., Preston, R. F., and Purser, A., Fabrication and Materials Evaluation of High Performance Aligned Ceramic Fiber-Reinforced Glass Matrix Composite, *Ceram. Eng. Sci. Proc.*, **8**[7-8] 815-21 (1987).

38. Hegeler, H. and Bruckner, R., Fiber-Reinforced Glasses: Influence of Thermal Expansion of the Glass Matrix on Strength and Fracture Toughness of the Composites, *J. Mater. Sci.*, **25**[11] 4836-46 (1990).

39. Shetty, D. K., Pascucci, M. R., Mutsuddy, B. C., and Wills, R. R., SiC Monofilament-Reinforced Si_3N_4 Matrix Composites, *Ceram. Eng. Sci. Proc.*, **6**[7-8] 632-45 (1985).

40. Xu, H. H. K., Ostertag, C. P., Braun, L. M., and Lloyd, I. K., Effect of Fiber Volume Fraction on Mechanical Properties of SiC-Fiber/Si_3N_4-Matrix Composites, *J. Am. Ceram.*

Soc., **77**[7] 1897-900 (1994).

Table I. Room Temperature Properties of Unidirectionally Reinforced CVD SiC_f/SAS Composites Hot Pressed at 1400°C, 27.6 MPa, 2h

Property	SCS-0/SAS #SAS 6-9-93	SCS-6/SAS #SAS 6-1-93
Measured		
Fiber volume fraction, V_f	0.24	0.31
Density, ρ, g/cm^3	2.99[a]	2.93
Elastic modulus[b], E, GPa	102 ± 10	122 ± 5
First matrix cracking stress[b], σ_y, MPa	231 ± 20	290 ± 40
First matrix cracking strain[b], ϵ_y, %	~0.22	~0.28
Ultimate strength[b], σ_u, MPa	265 ± 17	625 ± 50
Fiber/matrix ISS[c], τ_{debond}, MPa	17.5 ± 2.7	6.7 ± 0.7
Sliding frictional stress, $\tau_{friction}$, MPa	11.3 ± 1.6	4.2 ± 0.6
Calculated		
σ_y, MPa	365-429	432-494
Transition crack length, C_m, μm	625	886
σ_u, MPa		877

[a] ~98% of theoretical density
[b] From three point bend test
[c] From fiber push-out test

Table II. Influence of Fiber Content on Mechanical Properties of CVD SiC_f(SCS-6)/SAS Composites Measured in 3-Point Flexure [Hot Pressed 1400°C, 2 h, 27.6 MPa]

Composite #	V_f, %	σ_y, MPa	E_c, GPa	σ_u, MPa
---	0.0	130	70	---
SAS 10-6-93	15.8±0.2	163±3	124±7	477±26
SAS 9-7-93	20±0.5	211±35	139±8	531±27
SAS 8-6-93	35±1	332±43	216±14	861±33
SAS 9-13-93[a]	40±2	225±24	200±17	524±79

Average values for 4-5 test bars.

[a] Samples with V_f = 40% failed in shear. Other samples failed in tension.

Table III. Fiber-Matrix Interface Shear Strength and Sliding Frictional Stress Evaluated from Fiber Push-out for CVD SiC_f/SAS Composites [Hot Pressed 1400 °C, 2 h, 27.6 MPa]

Sample thickness, mm	Interface shear strength[a], τ_{debond}, MPa	Sliding frictional stress[a], $\tau_{friction}$, MPa
SCS-6/SAS Comp. [V_f = 0.31; SAS 6-1-93]		
1.31	6.7 (2.3)	3.7 (1.0)
1.74	6.6 (0.7)	4.4 (0.6)
1.84	7.0 (0.7)	4.2 (0.3)
2.57	6.6 (0.5)	4.3 (0.3)
SCS-0/SAS Comp. [V_f = 0.24; SAS 6-9-93]		
1.44	17.5 (2.7)[b]	11.3 (1.6)

[a]Mean value for 8-10 fibers. Values in parenthesis are standard deviation.

[b]Values in table are for fibers that debonded. However, one fiber showed τ_{debond} of 56.1 MPa which is not included in the average; some fibers did not debond up to a load of 40 N, the upper limit of the apparatus, resulting in $\tau_{debond} > 62$ MPa.

Table IV. Effect of Hot Pressing Time at 1450 °C, 24 MPa on Fiber/Matrix Interface Shear Strength, Sliding Frictional Stress and Flexure Strength of CVD SiC_f (SCS-6)/SAS Composites

Hot press time, min	σ_y, MPa[a]	σ_u, MPa[a]	τ_{debond}, MPa[b]	$\tau_{friction}$, MPa[b]
15 [#SAS 10-9-92]	201 ± 61	457 ± 51	4.77 ± 0.49	2.83 ± 0.40
30 [#SAS10-14-92]	280 ± 30	585 ± 67	6.13 ± 0.42	4.08 ± 0.25
60 [# SAS 12-15-92]	224 ± 16	590 ± 75	6.53 ± 0.16	4.15 ± 0.31
120 [#SAS 10-23-92]	223 ± 35	660 ± 40	7.78 ± 0.33	4.45 ± 0.46

[a]From three-point bend test
[b]From fiber push-out test; average for 10 fibers

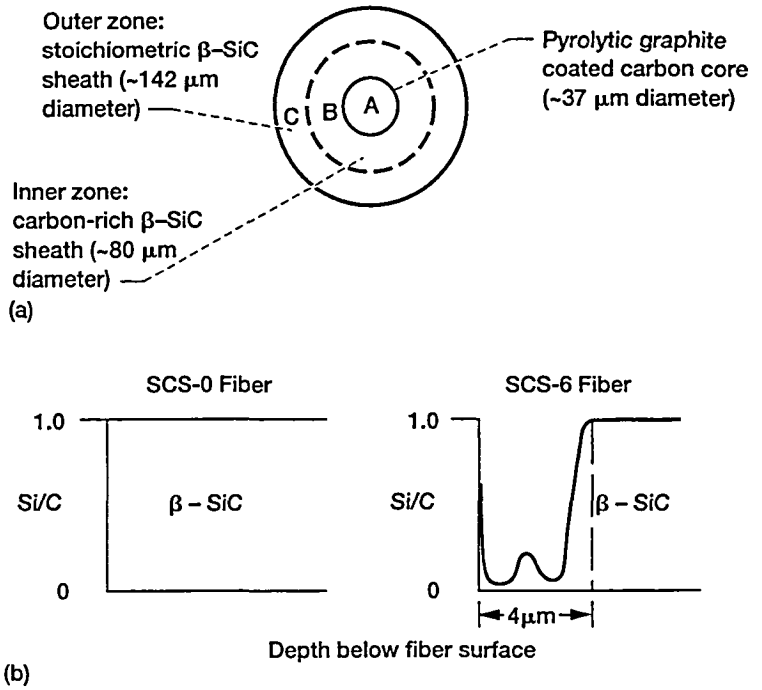

Figure 1.—Schematics showing cross-sections and surface regions of Textron CVD SiC SCS-0 and SCS-6 monofilaments. (a) Cross-section. (b) Surface region.

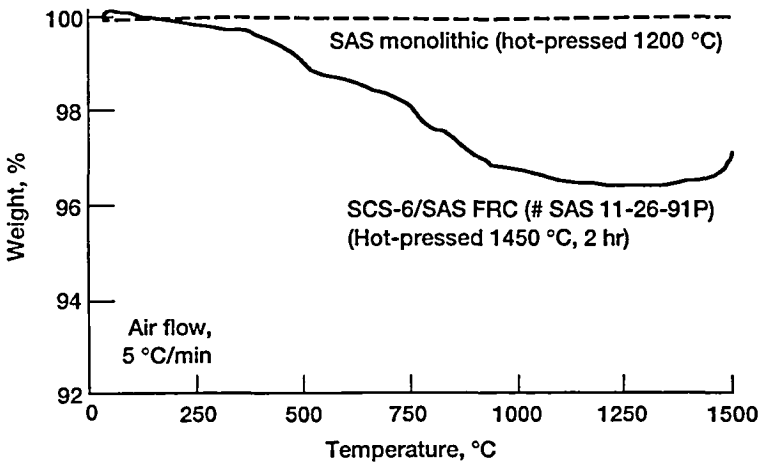

Figure 2.—TGA curves (recorded at a heating rate of 5 °C/min in flowing air) of SAS monolithic hot pressed at 1200 °C for 2 hr and SiC_f(SCS-6)/SAS composite (V_f = 0.3) hot pressed at 1450 °C for 2 hr.

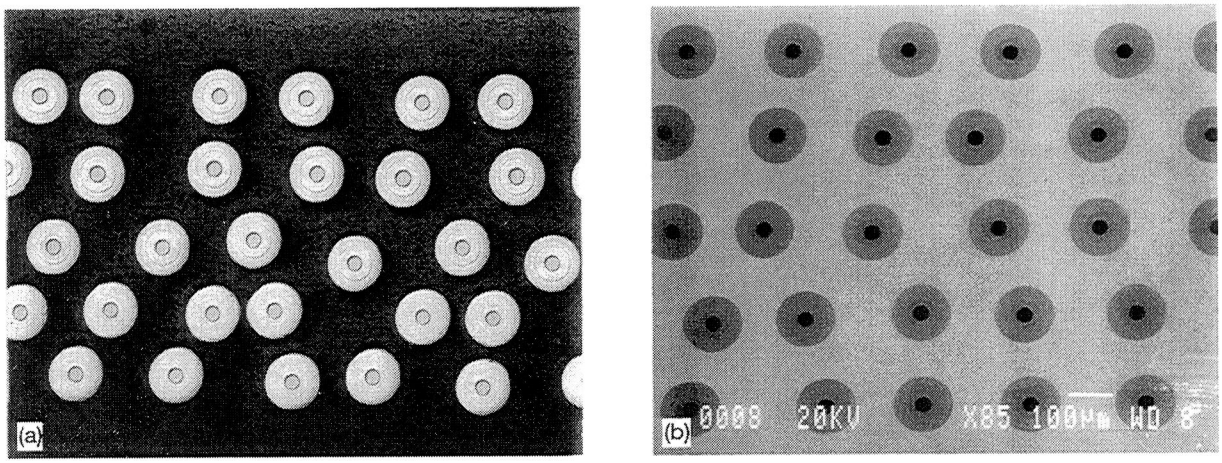

Figure 3.—Micrographs of polished cross-sections of unidirectional CVD SiC_f/SAS composites. (a) Optical micrograph of plasma etched SCS-6/SAS composite hot pressed at 1450 °C for 2 hr under 24 MPa. (b) SEM micrograph of SCS-0/SAS composite hot pressed at 1400 °C for 2 hr under 27.6 MPa, showing uniform fiber distribution.

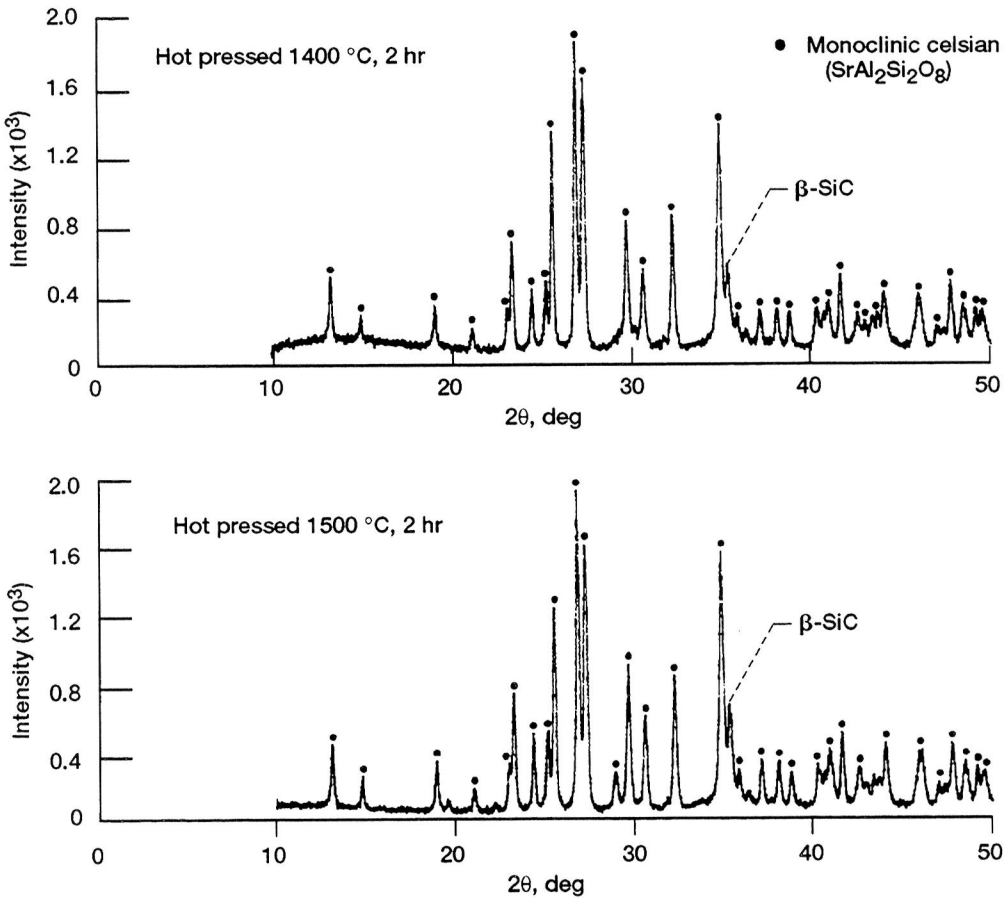

Figure 4.—Powder x-ray diffraction patterns of SCS-6/SAS composites hot pressed for 2 hr at 1400 °C or 1500 °C. The peak at 2θ = 35.6 is due to β-SiC. The remaining peaks correspond to monoclinic celsian.

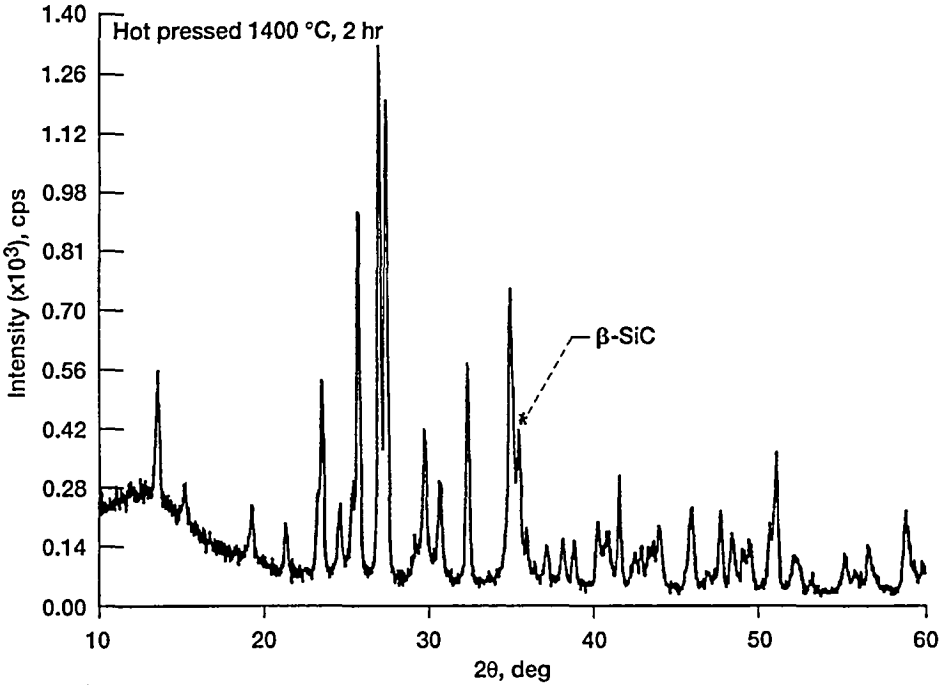

Figure 5.—Powder x-ray diffraction pattern of SCS-0/SAS composite hot pressed for 2 hr at 1400 °C at 27.6 MPa. The peak at 2θ = 35.6 is due to β-SiC. The remaining peaks correspond to monoclinic celsian.

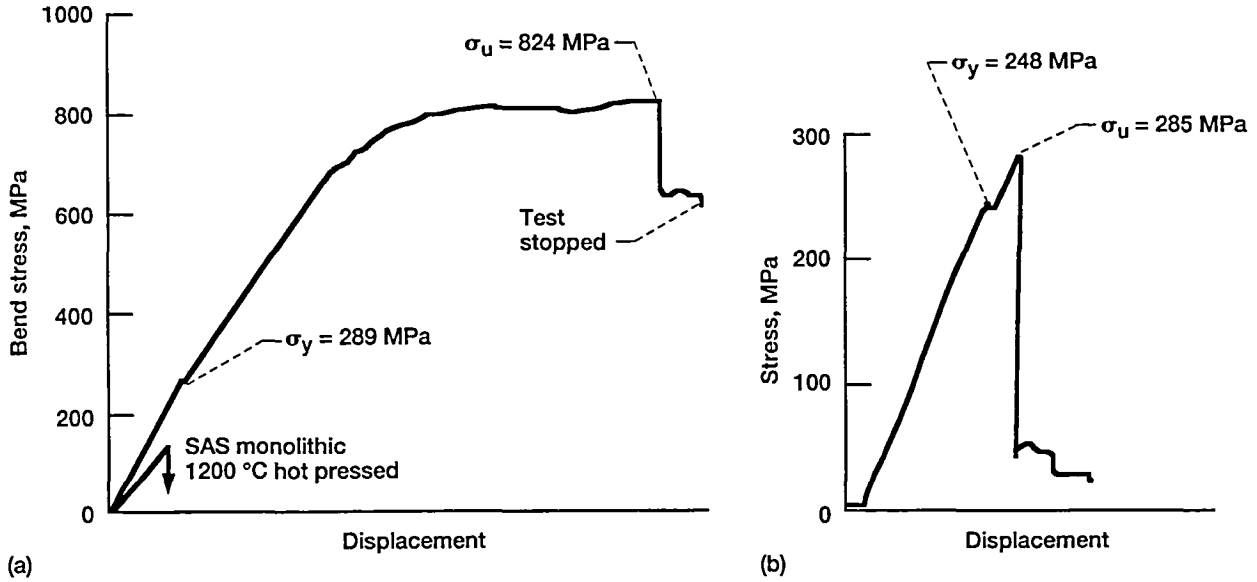

Figure 6.—Stress-displacement curves. (a) SAS monolithic hot pressed at 1200 °C for 2 hr under 24 MPa and a unidirectional SCS-6/SAS composite (V_f = 0.24) hot pressed at 1400 °C for 2 hr under 24 MPa. (b) A unidirectional SCS-0/SAS composite (V_f = 0.24) hot pressed at 1400 °C for 2 hr under 27.6 MPa. The monolithic ceramic was tested in four-point bending and the composites in three-point bending, respectively.

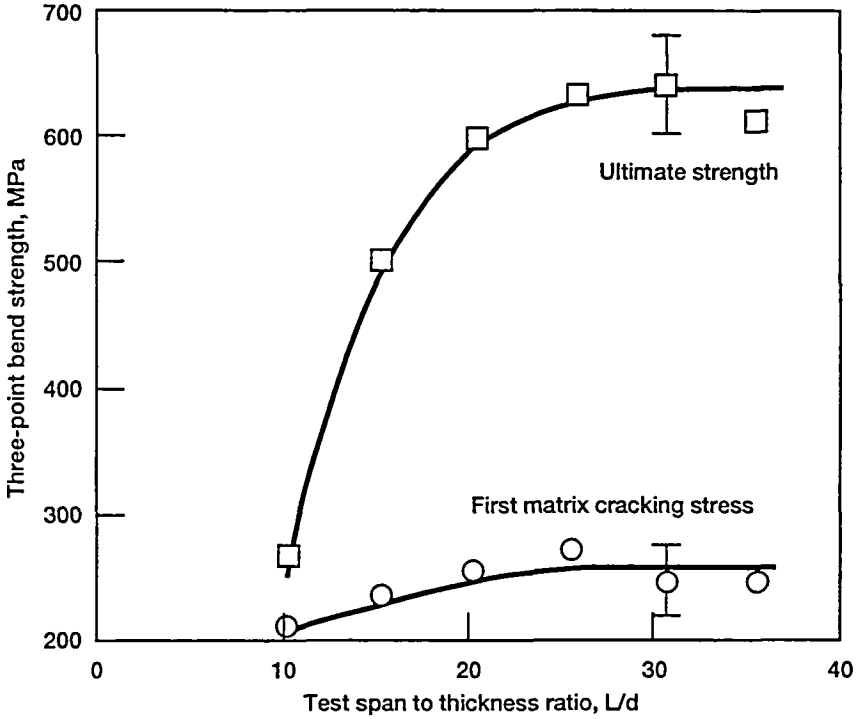

Figure 7.—Effect of test span length to sample thickness ratio (L/d) on first matrix cracking stress and ultimate strength, measured in three-point flexure, for a unidirectional SCS-6/SAS composite hot pressed at 1350 °C for 2 hr at 24 MPa; $V_f = 0.25$. One test/data point except for L/d = 32 where five specimens were tested.

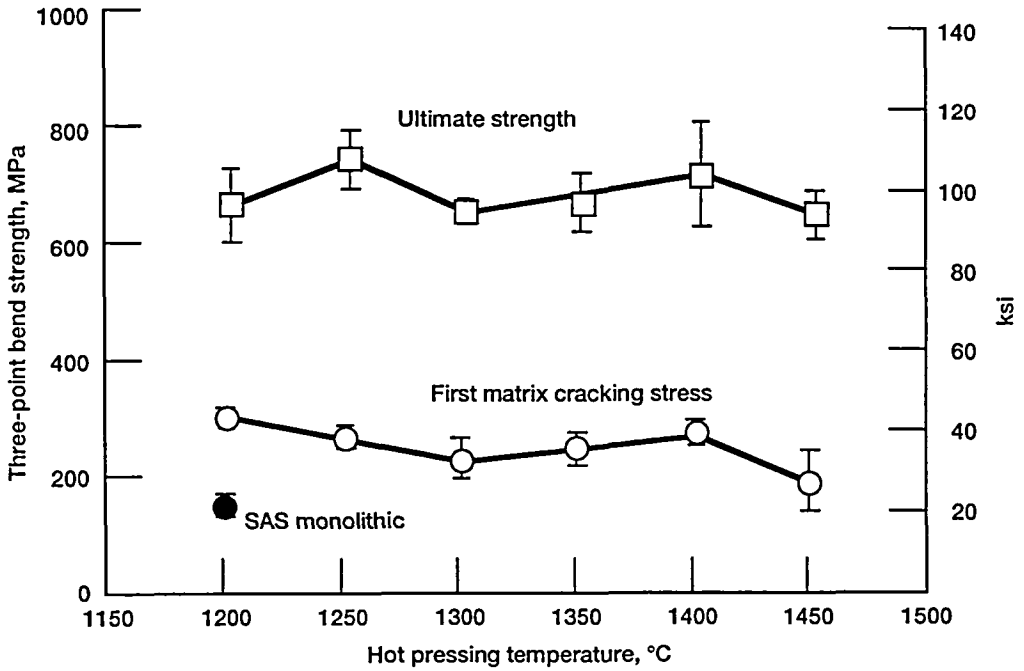

Figure 8.—Effect of hot pressing temperature on first matrix cracking stress and ultimate strength, measured at room temperature in three-point flexure, for a unidirectional CVD SiC_f(SCS-6)/SAS composite hot pressed for 2 hr at 24 MPa; $V_f = 0.25 \pm 0.01$. Also shown is the four-point bend strength of a SAS monolithic sample hot pressed at 1200 °C for 2 hr.

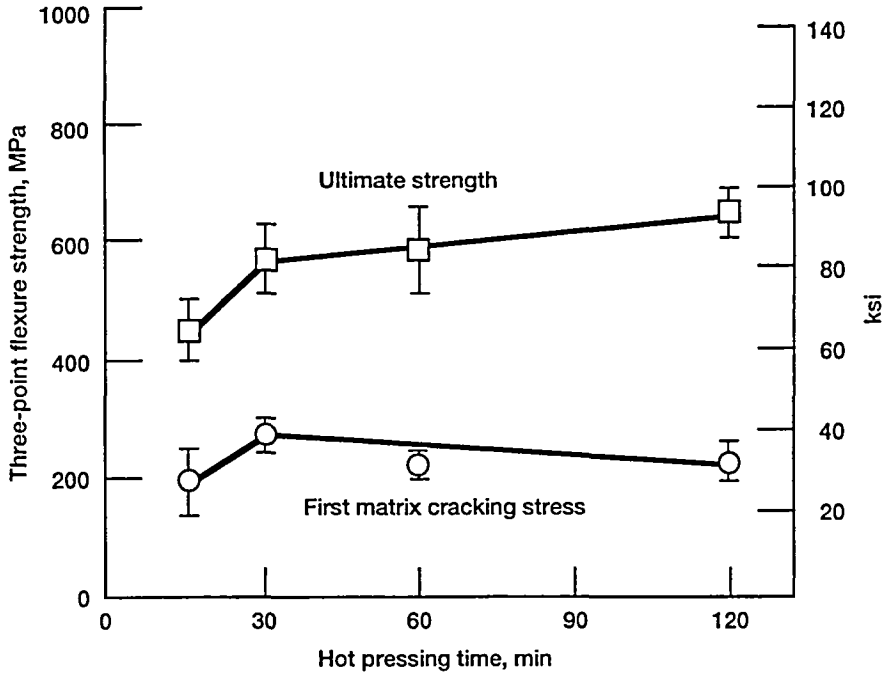

Figure 9.—Effect of hot pressing time on room temperature three-point flexural strength of unidirectional SCS-6/SAS composites hot pressed at 1450 °C at 24 MPa; $V_f = 0.24 \pm 0.01$. The lines drawn are only guide to the eyes.

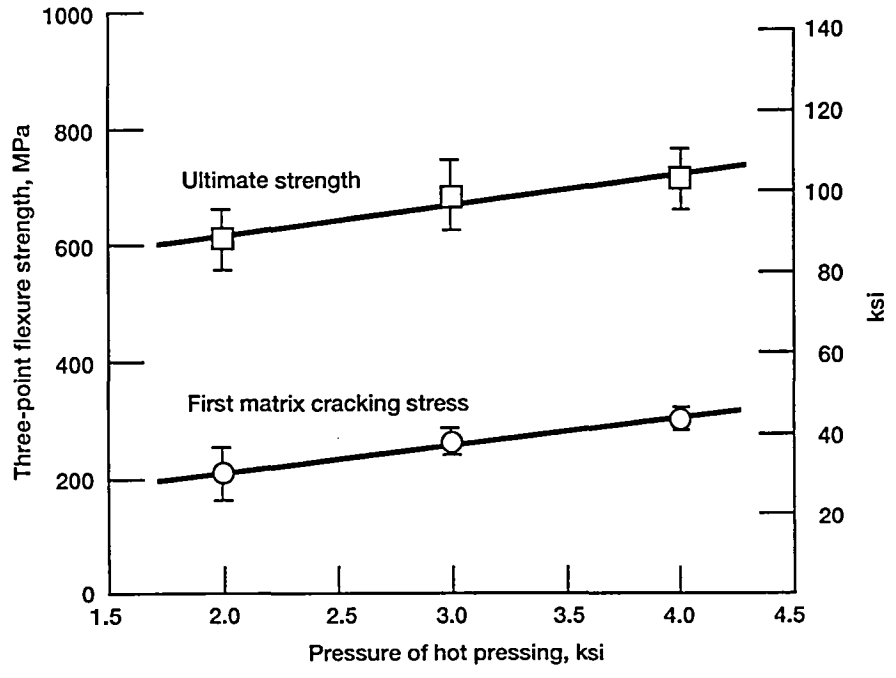

Figure 10.—Effect of hot pressing pressure on room temperature three-point flexural strength of unidirectional SCS-6/SAS composites hot pressed at 1450 °C for 2 hr; $V_f = 0.26 \pm 0.02$.

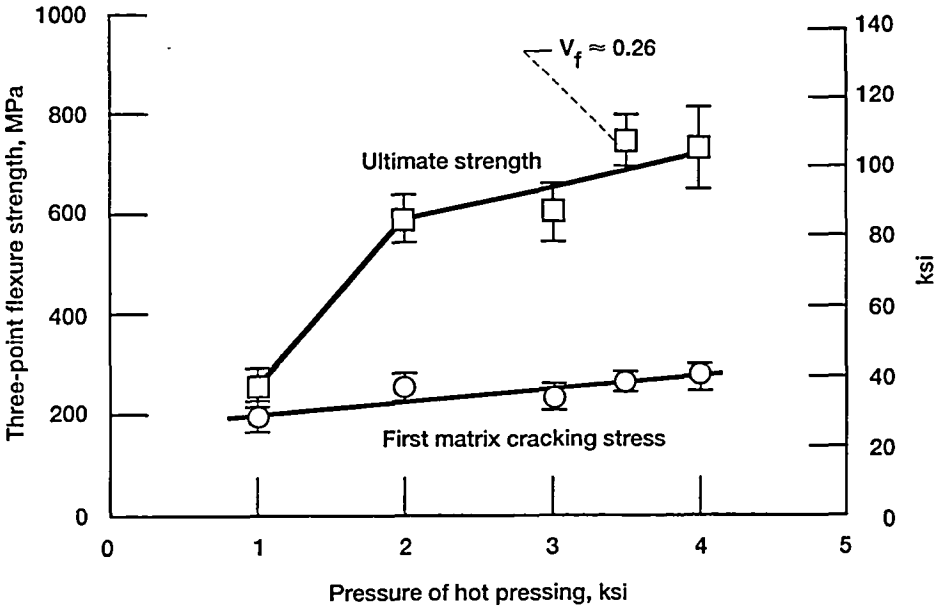

Figure 11.—Effect of hot pressing pressure on room temperature three-point flexural strength of unidirectional SCS-6/SAS composites hot pressed at 1250 °C for 2 hr; $V_f = 0.22 \pm 0.01$.

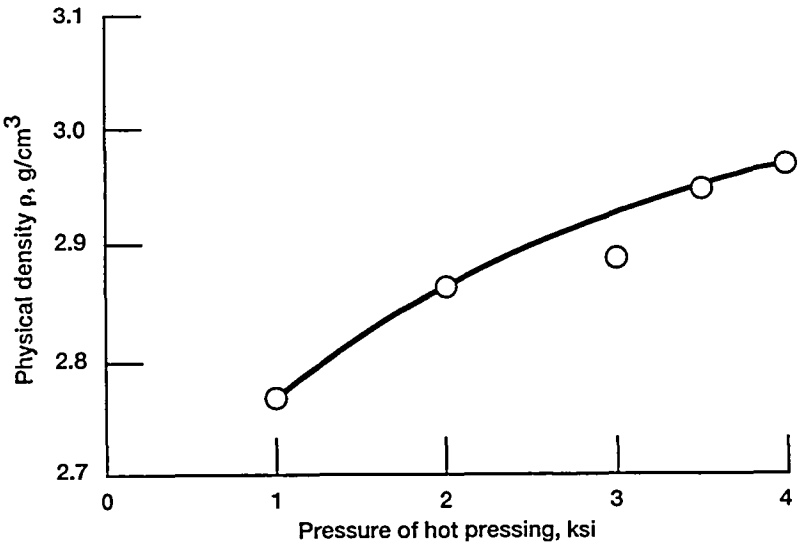

Figure 12.—Effect of hot pressing pressure on densities of unidirectional SCS-6/SAS composites hot pressed at 1250 °C for 2 hr; $V_f = 0.22 \pm 0.01$.

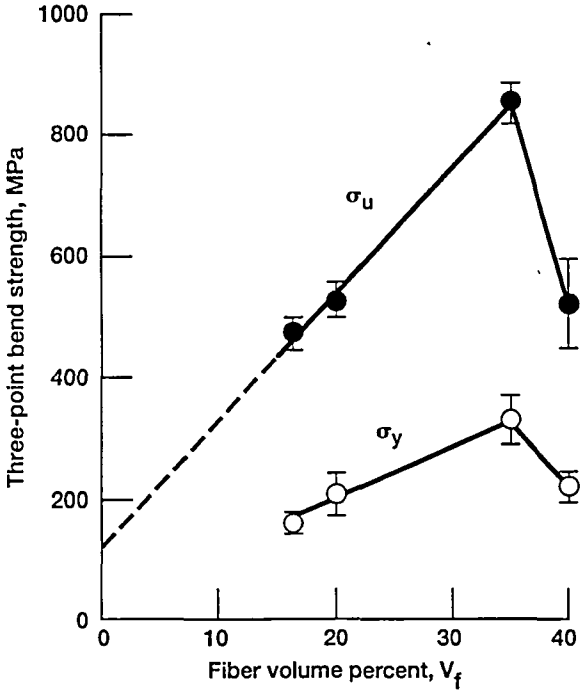

Figure 13.—Effect of fiber content on matrix microcracking stress and ultimate strength, measured in three-point flexure at room temperaure, for unidirectional CVD SiC_f(SCS-6)/SAS composites hot pressed at 1400 °C for 2 hr at 27.6 MPa.

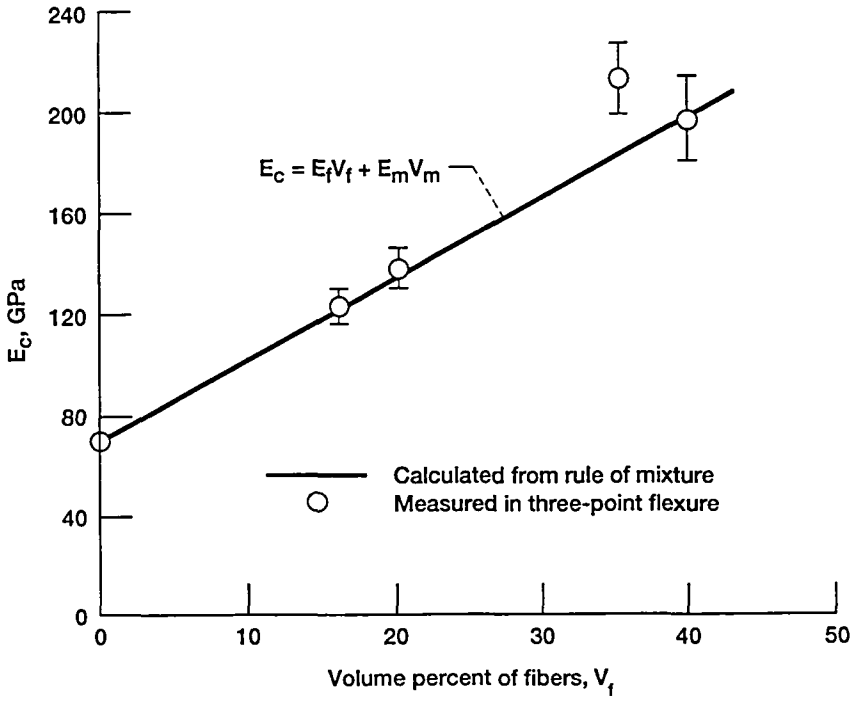

Figure 14.—Comparison of elastic modulus measured in three-point bend with those calculated from the rule-of-mixtures for unidirectional SCS-6/SAS composites with various fiber volume contents.

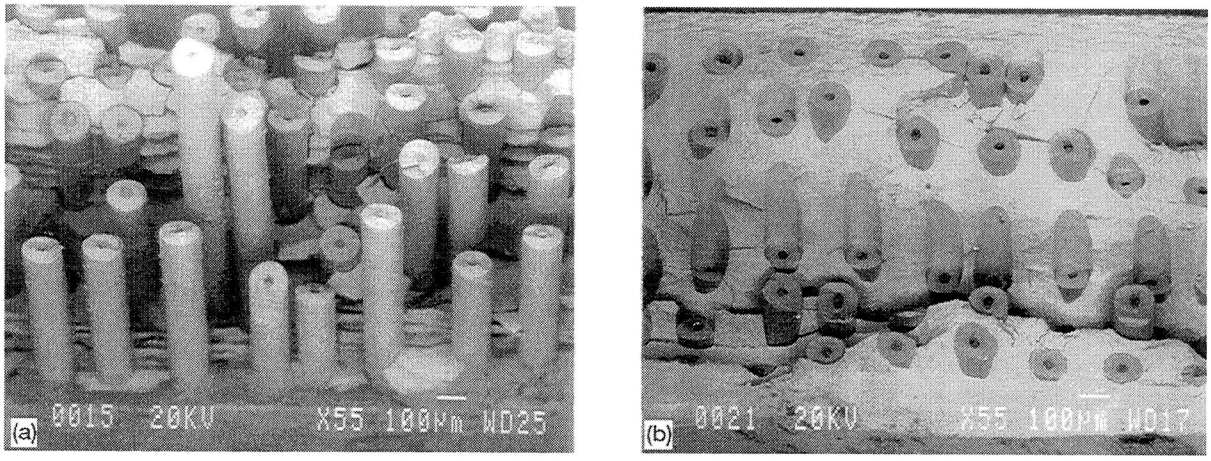

Figure 15.—SEM micrographs of fracture surfaces of unidirectional CVD SiC fiber reinforced SAS composites hot pressed at 1400 °C for 2 hr under 27.6 MPa. (a) SCS-6/SAS composite, V_f = 0.27, showing extensive fiber pullout. (b) SCS-0/SAS composite, V_f = 0.24, showing limited fiber pullout.

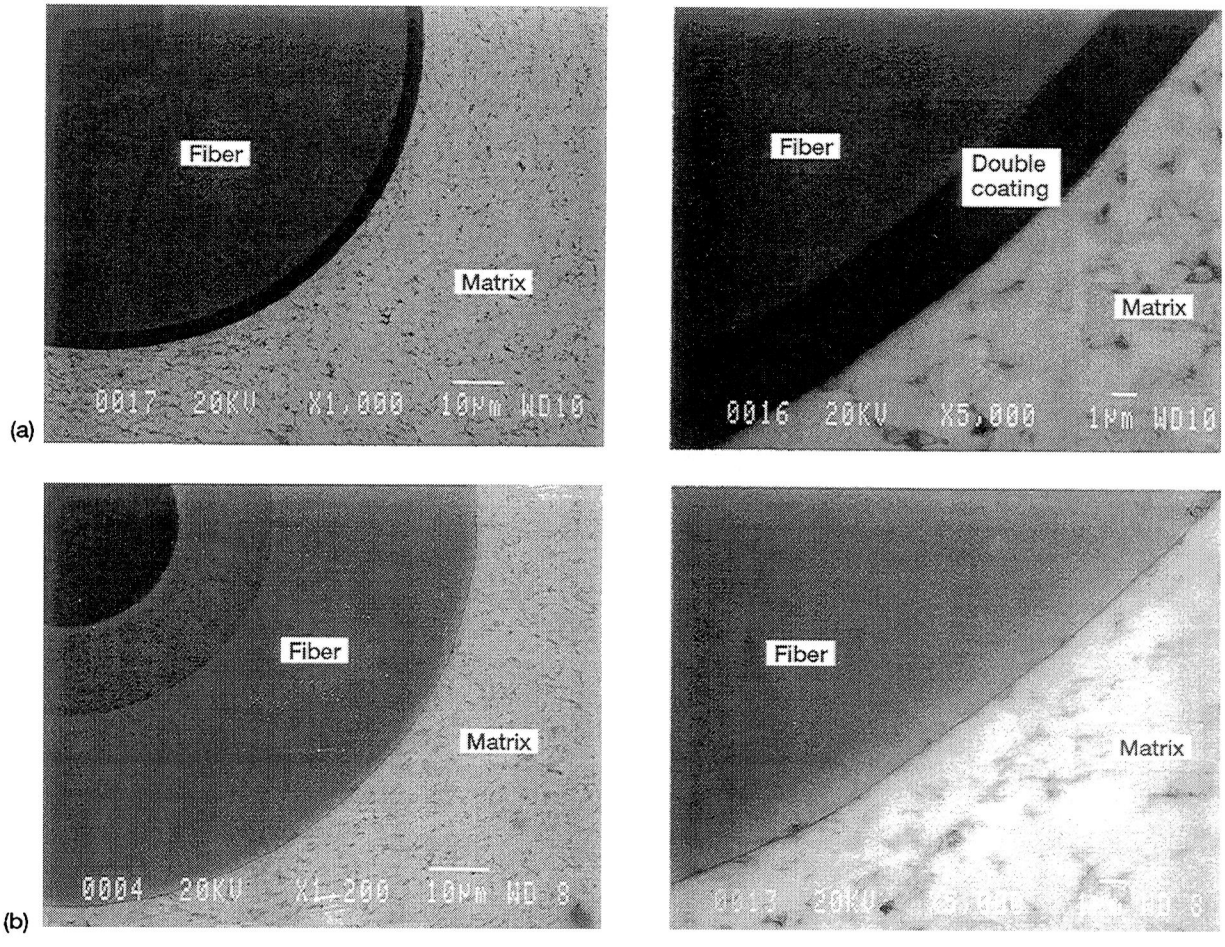

Figure 16.—SEM micrographs of polished cross-sections showing the fiber-matrix interface in unidirectional CVD SiC fiber reinforced SAS composites hot pressed at 1400 °C for 2 hr at 27.6 MPa. (a) SCS-6/SAS composite. (b) SCS-0/SAS composite.

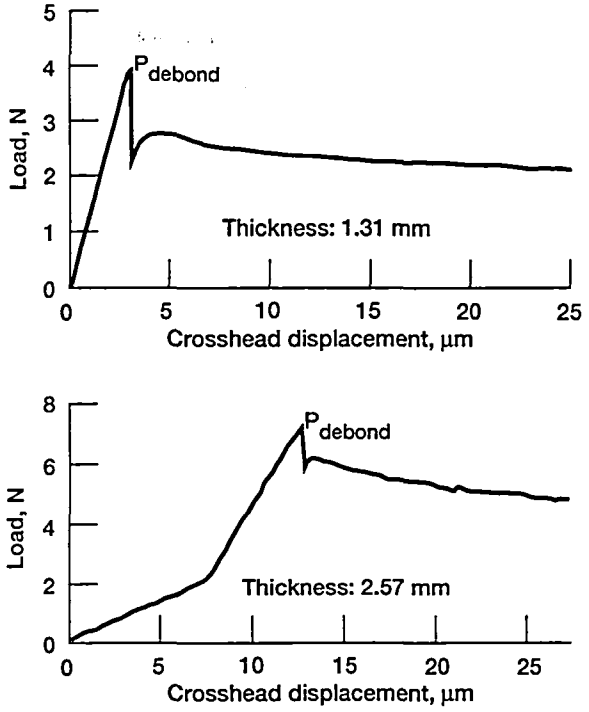

Figure 17.—Typical load vs. crosshead displacement curves recorded during fiber pushout in CVD SiC_f(SCS-6)/SAS composite hot pressed at 1400 °C for 2 hr at 27.6 MPa; for 1.31 and 2.57 mm thick samples.

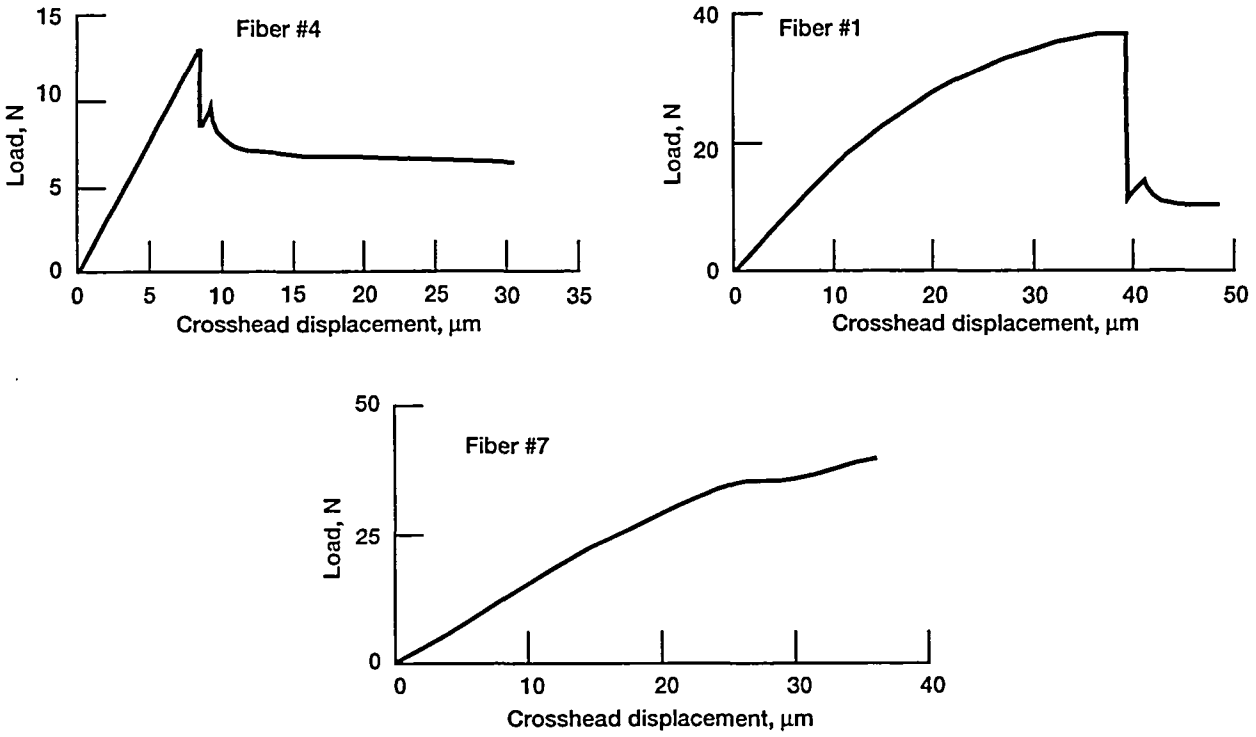

Figure 18.—Typical load vs. crosshead displacement curves recorded during fiber pushout in CVD SiC_f(SCS-0)/SAS composite hot pressed at 1400 °C for 2 hr under 27.6 MPa; sample thickness was 1.44 mm.

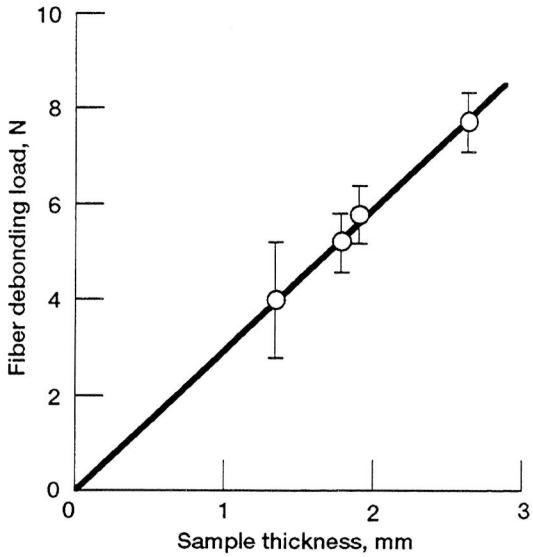

Figure 19.—Effect of sample thickness on fiber/matrix debonding load for CVD SiC_f(SCS-6)/SAS composite hot pressed at 1400 °C for 2 hr at 27.6 MPa; V_f = 0.31.

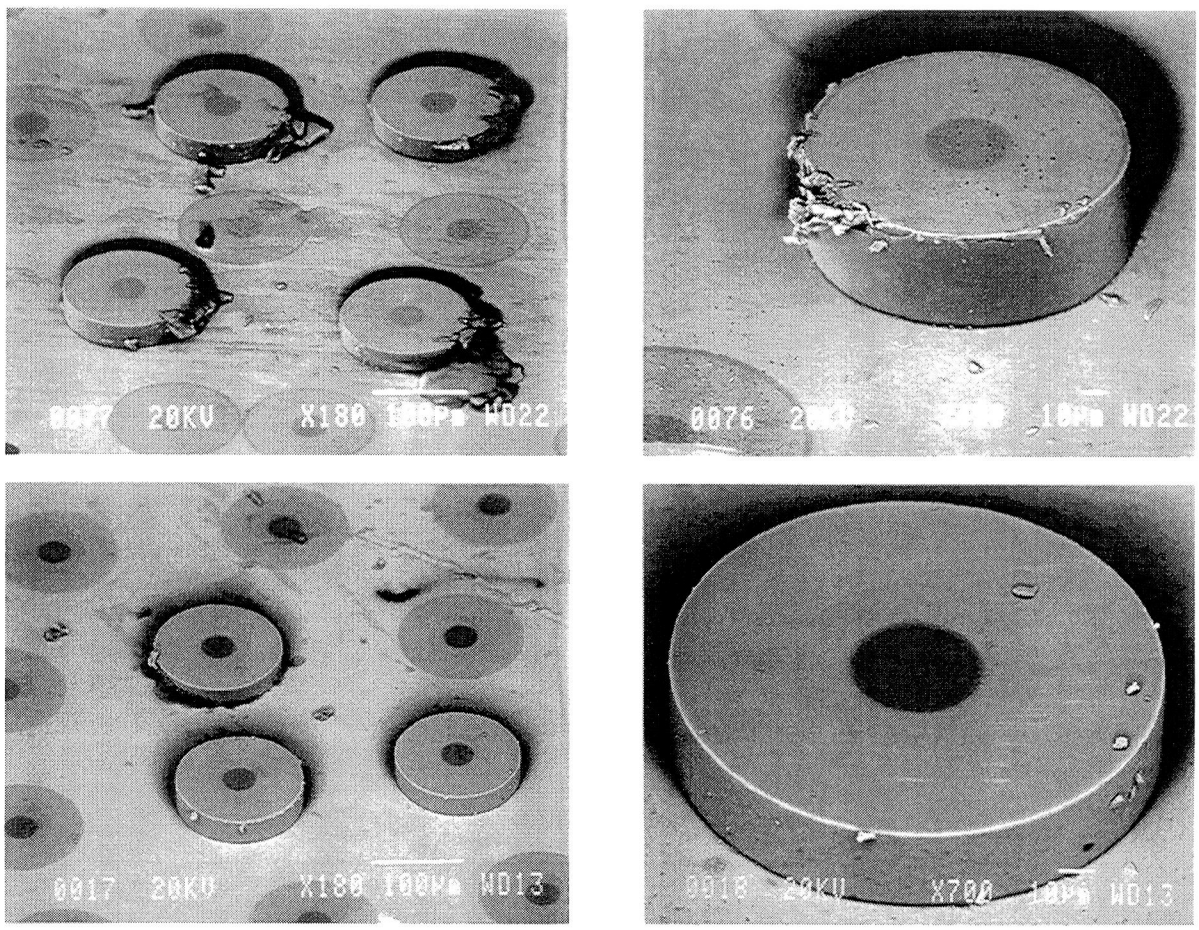

Figure 20.—SEM micrographs showing in-place and pushed out fibers in CVD SiC_f/SAS composites. (a) SCS-6/SAS composite hot pressed at 1500 °C for 2 hr at 24 MPa. (b) SCS-0/SAS composite hot pressed at 1400 °C for 2 hr under 27.6 MPa.

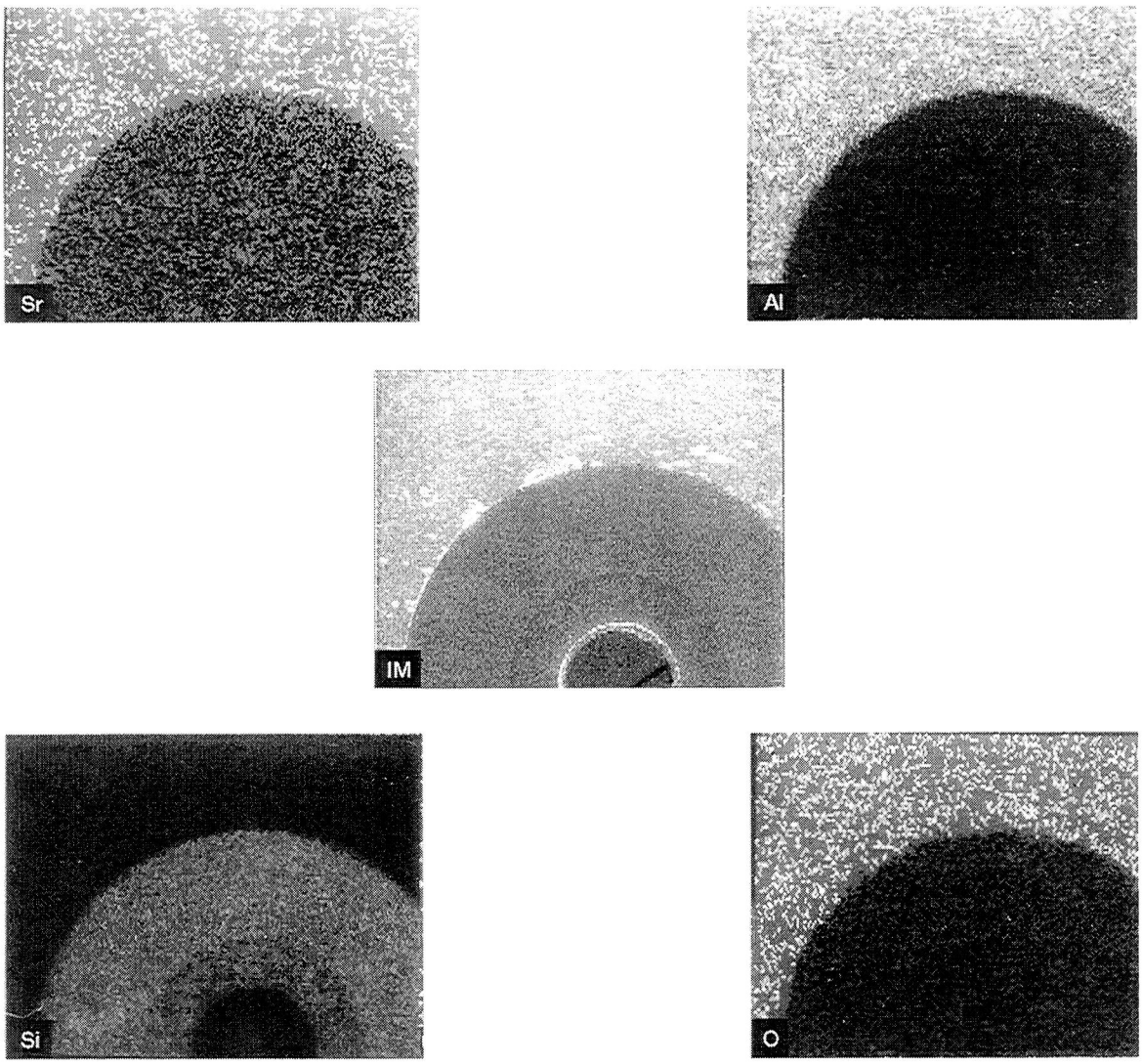

Figure 21.—SEM micrograph and x-ray maps of various elements at the fiber-matrix interface of the polished cross-section of a unidirectional CVD SiC_f(SCS-0)/SAS composite hot pressed at 1400 °C for 2 hr under 27.6 MPa.

REPORT DOCUMENTATION PAGE

Form Approved
OMB No. 0704-0188

1. AGENCY USE ONLY (*Leave blank*)	2. REPORT DATE	3. REPORT TYPE AND DATES COVERED
	August 1995	Technical Memorandum

4. TITLE AND SUBTITLE

CVD Silicon Carbide Monofilament Reinforced $SrO\text{-}Al_2O_3\text{-}2SiO_2$ (SAS) Glass-Ceramic Composites

5. FUNDING NUMBERS

WU-505-63-12

6. AUTHOR(S)

Narottam P. Bansal

7. PERFORMING ORGANIZATION NAME(S) AND ADDRESS(ES)

National Aeronautics and Space Administration
Lewis Research Center
Cleveland, Ohio 44135-3191

8. PERFORMING ORGANIZATION REPORT NUMBER

E-9767

9. SPONSORING/MONITORING AGENCY NAME(S) AND ADDRESS(ES)

National Aeronautics and Space Administration
Washington, D.C. 20546-0001

10. SPONSORING/MONITORING AGENCY REPORT NUMBER

NASA TM-106992

11. SUPPLEMENTARY NOTES

Responsible person, Narottam P. Bansal, organization code 5130, (216) 433-3855.

12a. DISTRIBUTION/AVAILABILITY STATEMENT

Unclassified - Unlimited
Subject Category 24

This publication is available from the NASA Center for Aerospace Information, (301) 621-0390.

12b. DISTRIBUTION CODE

13. ABSTRACT (*Maximum 200 words*)

Unidirectional CVD SiC fiber-reinforced $SrO.Al_2O_3.2SiO_2$ (SAS) glass-ceramic matrix composites have been fabricated by hot pressing at various combinations of temperature, pressure and time. Both carbon-rich surface coated SCS-6 and uncoated SCS-0 fibers were used as reinforcements. Almost fully dense composites have been obtained. Monoclinic celsian, $SrAl_2Si_2O_8$, was the only crystalline phase observed in the matrix from x-ray diffraction. During three point flexure testing of composites, a test span to thickness ratio of ~25 or greater was necessary to avoid sample delamination. Strong and tough SCS-6/SAS composites having a first matrix crack stress of ~300 MPa and an ultimate bend strength of ~825 MPa were fabricated. No chemical reaction between the SCS-6 fibers and the SAS matrix was observed after high temperature processing. The uncoated SCS-0 fiber-reinforced SAS composites showed only limited improvement in strength over SAS monolithic. The SCS-0/SAS composite having a fiber volume fraction of 0.24 and hot pressed at 1400°C exhibited a first matrix cracking stress of ~231±20 MPa and ultimate strength of 265±17 MPa. From fiber push-out tests, the fiber/matrix interfacial debonding strength (τ_{debond}) and frictional sliding stress ($\tau_{friction}$) in the SCS-6/SAS system were evaluated to be ~6.7±2.3 MPa and 4.3±0.6 MPa, respectively, indicating a weak interface. However, for the SCS-0/SAS composite, much higher values of ~17.5±2.7 MPa for τ_{debond} and 11.3±1.6 MPa for $\tau_{friction}$ respectively, were observed; some of the fibers were so strongly bonded to the matrix that they could not be pushed out. Examination of fracture surfaces revealed limited short pull-out length of SCS-0 fibers. The applicability of various micromechanical models for predicting the values of first matrix cracking stress and ultimate strength of these composites were examined.

14. SUBJECT TERMS	15. NUMBER OF PAGES
Composites; Celsian; Glass-ceramic; Mechanical properties; Interface; Micromechanical models	41
	16. PRICE CODE: A03

17. SECURITY CLASSIFICATION OF REPORT	18. SECURITY CLASSIFICATION OF THIS PAGE	19. SECURITY CLASSIFICATION OF ABSTRACT	20. LIMITATION OF ABSTRACT
Unclassified	Unclassified	Unclassified	

National Aeronautics and
Space Administration

Lewis Research Center
21000 Brookpark Rd.
Cleveland, OH 44135-3191